The β_2-adrenergic receptor is a molecular switch for neuroendocrine transdifferentiation of prostate cancer cells

Peder R. Braadland [1,2], Håkon Ramberg [1], Helene H. Grytli [1], Alfonso Urbanucci [1,3,4], Heidi K. Nielsen [1,2], Ingrid J. Guldvik [1], Andreas Engedal [1], Kirsi Ketola [5], Wanzhong Wang [6], Aud Svindland [2,7], Ian G. Mills [3,8,9], Anders Bjartell [10,11], Kristin A. Taskén [1,2]

[1] Department of Tumor Biology, Institute for Cancer Research, Oslo University Hospital, Oslo, Norway
[2] Institute of Clinical Medicine, University of Oslo, Oslo, Norway
[3] Centre for Molecular Medicine Norway, Nordic EMBL Partnership, University of Oslo, Oslo, Norway
[4] Dept. Of Core Facilities, Institute of Cancer Research, Oslo University Hospital, Norway
[5] Institute of Biomedicine, University of Eastern Finland, Kuopio, Finland
[6] Clinical Pathology/cytology, Karolinska University Hospital, Stockholm, Sweden
[7] Department of Pathology, Oslo University Hospital, Oslo, Norway
[8] Movember FASTMAN Centre of Excellence, Centre for Cancer Research & Cell Biology, Queen's University Belfast, Belfast, UK
[9] Nuffield Department of Surgical Sciences, University of Oxford, Oxford, UK
[10] Department of Urology, Skåne University Hospital, Malmö, Sweden
[11] Department of Translational Medicine, Division of Urological Cancers, Lund University, Malmø, Sweden

Running title: ADRB2 induces neuroendocrine transdifferentiation

Keywords: neuroendocrine transdifferentiation, castration resistant prostate cancer, neuroendocrine prostate cancer, lineage plasticity, neurite outgrowth, β2-adrenergic receptor, ADRB2, NEPC, CRPC, SCPC

Corresponding author: Kristin A. Taskén, Department of Tumor Biology, Institute for Cancer Research, Oslo University Hospital, P.O.Box 4953 Nydalen, NO-0424 Oslo, Norway. Telephone: +47-22781878. E-mail: k.a.tasken@medisin.uio.no

Word count abstract: 249

Word count text: 6355

Total number of figures and tables: 6 figures, 9 Supplementary figures, 2 Supplementary tables

The authors declare no potential conflicts of interest

Abstract

The incidence of treatment-related neuroendocrine (NE) prostate cancer (t-NEPC) is rising as more potent drugs targeting the androgen signaling axis are clinically implemented. Neuroendocrine transdifferentiation (NEtD), an putative initial step in t-NEPC development, is induced by androgen deprivation therapy (ADT) or anti-androgens, and by activation of the β_2-adrenergic receptor (ADRB2) in prostate cancer cell lines. Thus, understanding whether ADRB2 is involved in ADT-initiated NEtD may assist in developing treatment strategies that can prevent or reverse t-NEPC emergence, thereby prolonging therapeutic responses.

Here we found that in primary, treatment-naïve prostate cancers, ADRB2 mRNA was positively correlated with expression of luminal differentiation markers, and ADRB2 protein levels were inversely correlated with Gleason grade. ADRB2 mRNA was upregulated in metastatic prostate cancer, and progressively downregulated during androgen deprivation therapy (ADT) and t-NEPC emergence. In androgen-deprivated medium, high ADRB2 was required for LNCaP cells to undergo NEtD, measured as increased neurite outgrowth and expression of neuron differentiation and NE genes. ADRB2 overexpression induced an NE-like morphology in both AR positive and -negative prostate cancer cell lines. ADRB2 downregulation in LNCaP cells increased canonical Wnt signaling, and GSK3α/β inhibition reduced the expression of neuron differentiation and NE genes. In LNCaP xenografts, more pronounced castration-induced NEtD was observed in tumors derived from high than low-ADRB2 cells.

In conclusion, high ADRB2 expression is required for ADT-induced NEtD, characterized by ADRB2 downregulation and t-NEPC emergence.

Implications: This data suggest a potential application of β-blockers to prevent cancer cells committed to a neuroendocrine lineage from evolving into t-NEPC.

Introduction

Androgen-deprivation therapy (ADT), involving surgical or chemical castration with agonists or antagonists of luteinizing hormone-releasing hormone (LHRH), remains the pillar in treatment of metastatic hormone sensitive prostate cancer (PCa). The majority of patients initially respond due to innate tumoral androgen dependence, but treatment resistance predictably develops as castration-resistant prostate cancer (CRPC) (1). Despite the introduction of second-line androgen receptor pathway inhibitors (ARPIs) such as abiraterone (ABI), enzalutamide (ENZ) and apalutamide, which have offered a survival benefit (2), CRPC remains a lethal disease.

Recent studies indicate that increasing use of existing and novel ARPIs is introducing new challenges in the management of advanced PCa: More potent AR pathway inhibition is believed to impose a therapeutic pressure on PCa cells, which can promote adaptation and selection for traits that alleviate tumoral androgen dependence (3, 4). In recent years, novel CRPC subtypes displaying AR negativity and/or low reliance on AR signaling have gained attention due to their increased incidence in the post-ABI/ENZ era (3, 5, 6). These subtypes are believed to develop through lineage plasticity, whereby PCa cells escape androgen dependence and sensitivity through relying on alternative pathways for sustained survival (7, 8), and may display stem cell/basal like features and/or neuroendocrine differentiation (9).

A significant proportion of androgen-independent CRPCs display neuroendocrine differentiation, and are commonly termed treatment-related neuroendocrine prostate cancer (t-NEPC). As many as 13-27 % of CRPC patients have tumors which display NEPC (3, 10, 11), and almost 80 % of metastatic CRPCs show at least focal neuroendocrine (NE) features (12). Treatment-related NEPC is more frequently observed in tumors challenged with ARPIs, but a significant proportion of ABI/ENZ-naïve, ADT-treated tumors also develop t-NEPC (11). Molecularly, NEPCs typically feature positive immunohistochemical staining with NE-markers, low or negative AR expression and disproportionally low or negative prostate-specific antigen (PSA) expression. Clinically, NEPCs commonly metastasize to visceral tissue, form osteolytic bone metastases, are very aggressive and not responsive to androgen signaling targeted therapies (5, 13). These molecular and clinical features resemble the highly aggressive *de novo* small-cell carcinoma of the prostate, which accounts for less than 1 % of all primary PCa diagnoses.

A model where NE cells present in advanced PCa are clonally selected during ADT has been suggested at least in part to explain the emergence of NEPC (14). However, compelling evidence from both preclinical models and genetic studies on autopsy-derived metastases (4, 15-17) suggest that these cells divergently transdifferentiate from adenocarcinoma cells during androgen-targeting therapy modalities.

Adrenergic stimulation, like androgen withdrawal, has been shown to induce NE-like features in PCa cell lines (18, 19). In the present study, we have investigated the role of ADRB2 in PCa progression to NEPC by analyses of clinical specimens and functional assays on preclinical model systems with modulated ADRB2 levels. We find that ADRB2 acts as a molecular switch for NEtD in PCa, and is progressively lost during tumor dedifferentiation and emergence of therapy resistance.

Patients, material and methods

Tissue microarray and immunohistochemistry

The tissue microarray (TMA) includes radical prostatectomy tissue from 122 patients treated at Skåne University Hospital between 1999 and 2002 (20). The TMA was immunohistochemically stained as described previously (21) with an anti-ADRB2 primary antibody (MC2656; MBL Int., Woburn, MA) in a 1:4000 dilution. Time of biochemical recurrence (BCR) was defined as the first date of two consecutive rises in PSA above nadir (>0.2 ng/mL).

Manual scoring of the ADRB2 antibody staining on a scale from 1-3 was performed by two experienced uropathologists (WW, AS). The most profound Gleason grade in each spot was also reported. In cases with more than one cancerous spot from an individual patient, the staining intensity for the spot(s) with the highest Gleason grade was chosen for further analysis. All patients included on the TMA provided informed consent. The study was approved by the Regional Committees for Medical and Health Research Ethics (434-04153,S-04153c, 2009/373,09/00450-2/bso 2009/1028), Oslo University Research Support Unit (2011/3286) and by the Regional Ethical Review Board at Lund University, Sweden (approval number DN. 445-07).

Whole sections of fresh-frozen paraffin-embedded xenograft tumors were stained with an anti-ADRB2 antibody (1:4000) as described above. Staining procedures for anti-Tubulin β3 (TUBB3; 1:800; 801201, Nordic BioSite; Täby, Sweden) and anti-CD31 (1:50; ab28364, Abcam) are detailed in Supplementary materials and methods. Whole tumor section brightfield 10X scans were acquired using an AxioScan Z1 (Carl Zeiss, Oberkochen, Germany), and were imported to ImageJ. Staining-positive areas were measured by altering threshold and related to the total tumor area, excluding adjacent mouse stroma.

Cell lines and reagents

Prostate cancer cell lines LNCaP, VCaP and PC-3 were purchased from ATCC (Rockville, MD). All cells were maintained in RPMI 1640 (#R0883; Sigma; St. Louis, MO) with 10 % fetal calf serum (FCS - androgen-proficient medium; #F7524; Sigma) , 100 units/ml penicillin and 50 mg/ml streptomycin (#P4458; Sigma), and 1 % Alanyl-Glutamine (#G8541; Sigma) at 37^{o}C with an atmosphere of 5 % CO_2 and humidified air. In experiments involving androgen depletion, RPMI 1640 was replaced with phenol red-free RPMI 1640 (#32404014; Thermo Fisher; Waltham, MA), and FCS was replaced with 2 % charcoal-stripped serum (#A3382101; Thermo Fisher). Stable ADRB2 knockdown was performed as previously described (21), although here with an additional stable knockdown cell line (LNCaP shADRB2-3; insert sequence gaagtttacatcctcctaat), yielding a total of three shADRB2 and one shCtrl cell line. Stably transfected cells were kept in culture medium supplied with 200 µg/ml G418 sulphate

(#10131-027; Thermo Fisher). Cell IDs of VCaP, PC-3, parental LNCaP, LNCaP shADRB2 and shCtrl cell lines were verified using the STR PowerPlex16 System (Promega; Madison, WI), and the cells were routinely checked for mycoplasma infections. The GSK3α/β inhibitor, CHIR99012, was ordered from Selleckchem (#S2924; Huston, TX). MSAB (#SML1726), (±) isoproterenol (#I5627), propranolol (#P0884-1G) and forskolin (F6886) were purchased from Sigma.

Semi-Quantitative Real-Time RT- PCR

Total RNA was extracted using the TRIzol reagent (#15596018; Thermo Fisher) following the manufacturers' protocol (Invitrogen; Carlsbad, CA). A total of 100 ng of total RNA was used with the qScript™ One-Step qRT-PCR Kit (Quanta bio; Beverly, MA) as previously described (21). The primer sequences are listed in Suppl. Material and Methods. ALAS1 or POLR2A mRNA expression were used for reference. To display relative gene expression the $\Delta\Delta C_t$ method was used.

DNA Microarray

The integrity of extracted RNA was assessed using the 2100 Bioanalyzer (Agilent; Santa Clara, CA). A total of 500 ng RNA was amplified and labeled according to the TotalPrepTM RNA amplification kit protocol (Illumina; San Diego, CA), and concentrations were measured using the NanoDrop spectrophotometer (Thermo Fisher), and quality and size distributions were assessed using the 2100 Bioanalyzer. A total of 750 ng of biotin-labeled cRNA was hybridized to Illumina's HumanHT-12 v4 Expression BeadChip according to the manufacturer's protocol. Signal intensities were extracted using iScan software (Illumina), and raw data were quantile normalized and missing values imputed. The procedure was performed at the Genomics Core Facility Oslo University Hospital and Helse Sør-Øst (The Norwegian Radium Hospital, Oslo, Norway). The microarray data have been deposited at in NCBI's Gene Expression Omnibus (GEO (22)) repository and is accessible through series accession number GSE130204.

Protein extraction and Western blot analysis

The cells were harvested, lysed in whole cell buffer (21), and centrifuged at 16,000 g for 20 min. The NE-PER Nuclear and Cytoplasmic Extraction Reagents (#78833; Thermo Fisher) were used for fractionation of cells. Western blots were prepared and visualized as previously reported (21). Antibodies and their dilutions are listed in Supplementary material and methods. Where predicted molecular weights were similar for two or more antibodies, the same set of protein extracts were probed on separate gels.

ADRB2 radioligand binding assay

Cell membrane fractions from shCtrl and shADRB2 cells were prepared as described in (23). A radioligand binding assay was used to measure the ADRB2 protein binding activity as previously described (23, 24).

Neurite outgrowth measurements

For manual neurite length measurements, at least two representative regions of the images containing cells with similar aggregation and confluence were analyzed from ≥3 independent experiments. Measurement of the length of all neurites present in the captured, representative fields was performed using the NeuronGrowth plug-in in ImageJ (25) and was related to the manually counted number of cells in each field. Phase-contrast light microscopy images were acquired with the IncuCyte live-cell analysis system equipped with a 10X objective (ESSEN Bioscience; Ann Arbor, MI) or an IX81 microscope (Olympus; Tokyo, Japan). Automatic neurite length and branch points per cell (mm^2) quantifications were performed using the NeuroTrack Software module in six technical replicates of representative fields acquired on the IncuCyte S3 imaging system equipped with a 10X objective from ≥3 independent experiments.

ADRB2 overexpression experiments

The pcDNA3 Flag beta-2-adrenergic-receptor (pADRB2) containing the full length ADRB2 gene and a Flag-tag was a kind gift from Finn Olav Levy and Robert Lefkowitz (#14697; Addgene; Watertown, MA) (26). A non-expressing/empty pcDNA3.1/Zeo vector (pEmpty; #V860-20; Invitrogen) was used as transfection control. LNCaP parental, shCtrl and shADRB2, PC-3 and VCaP cells were transfected for 48h using XtremeGene HP DNA transfection reagent (#06366236001; Sigma) under androgen-proficient conditions.

Luciferase assay

In brief, cells were transfected using the Dharmafect Duo reagent (#T-2010-0; Dharmacon; Lafayette, CO). The plasmid pGL4.49 luc2P/TCF-LEF RE/Hygro (#E4611; Promega), containing eight copies of the TCL-LEF response elements was used to asses β-catenin-mediated transcriptional activity. A plasmid without the TCF-LEF response elements, pGL.49 luc2P/minP/Hygro (#E8451; Promega), was used as control. The pEZX-PG04 vector expressing SEAP (GeneCopoeia, Rockville, MD) was used to normalize for differences in transfection efficiency. The secreted alkaline phosphatase (SEAP) activity in medium samples was measured 24 or 48 hours after transfection using the Secrete-Pair Dual Luminescence Assay kit (#SPDA-D100; GeneCopoeia) on a Victor Wallac Spectrophotometer (PerkinElmer; Waltham, MA). To determine intra-cellular luciferase activity, cells were lysed in 1X Reporter Lysis buffer (#E397A; Promega), the supernatant mixed with Luciferase Assay Reagent

(#E152A; Promega) and the activity measured on a TD-20/20 luminometer (Turner Designs; Sunnyvale, CA).

Animal studies

Fifty-eight in-house bred, 4 weeks old male NOD-SCID gamma/null mice weighing 28.2±4 g were administered 0.03 mg/ml testosterone (#NA-151 Sigma) in drinking water one week prior to subcutaneous injection into the hind flank with $2x10^6$ cells of shCtrl (n=30), shADRB2-2 (n=13) or shADRB2-2 (n=15). Tumor volumes were assessed as described in (21). Time to take was defined as the time to the first measurement of the first two consecutive measurements of a palpable tumor. The mice were surgically castrated, and following termination, tumors were harvested and fresh-frozen and paraffin-embedded for IHC analyses. The experiment was approved by the National Animal Research Authority (FOTS ref. 7132) and was performed according to regulations of the Federation of European Laboratory Animals Science Association.

In silico analyses on published datasets

Median RNA-seq RNA expression values and clinicopathological data from Neuroendocrine Prostate Cancer (Trento/Cornell/Broad 2016, hereby called NEPC WCM) (4) were downloaded from cBioPortal (27, 28). Median expression values were scale normalized in R v3.4.3. Gene expression values and clinicopathological data from the Fred Hutchinson CRC (FHCRC; expression microarray) (29) and the Stand Up To Cancer/PCF Dream Team (SU2C/PCF; RNA-seq) 2015 (RPKM) (30) and 2019 (FPKM) (31) cohorts were downloaded from cBioPortal using the CDGSR package in R. Hierarchical clustering (Ward's method) and and heatmaps were generated using the pheatmap package in R. Where more than one sample was present for a patient, the samples were analyzed individually. Scale-normalized gene expression levels were downloaded from GSE35988 (GPL6848 and GPL6480) (32) and GSE41193 (16) using the GEOquery package in R from GEO. Quantile-normalized ADRB2 expression levels in cell lines was acquired from data deposited under GSE25183 (33). Gene set enrichment analyses were performed using DAVID v6.7 Functional Annotation (34).

Statistics

For cell line studies, two-sided Student's t-test was applied to test for statistical significance, and error bars depict standard error of the mean (SEM). The Shapiro-Wilk test was used to test normality. For animal experiment data, statistical significance was calculated using Wilcoxon rank sum tests or t-tests where indicated. Spearman correlation (*rho*) was applied to evaluate gene expression correlations. Wilcoxon rank sum tests were used to evaluate differences in ADRB2 gene expression in clinical datasets, assuming non-normal distributions determined by Shapiro-Wilk tests. For our microarray analysis, differential gene expression was assessed by significance analysis of microarrays

(SAM) comparing mRNA levels between shCtrl and shADRB2-2 and -3 LNCaP cells. A false discovery rate (FDR) of less than 0.05 was considered statistically significant.

Cox proportional hazards modeling was used for multivariable survival analyses. Kendall's tau-b correlation analysis was performed to evaluate correlations between Gleason grade and ADRB2 and AR staining intensities. Statistics were performed using STATA version 15 and R v3.4.3. A two-sided *P*-value of < 0.05 was considered statistically significant for all analyses.

Results

ADRB2 is associated with luminal differentiation

Immunohistochemical staining of a TMA consisting of specimens from 76 radical prostatectomies with an anti-ADRB2 antibody showed high ADRB2 levels in differentiated and low levels of ADRB2 in poorly differentiated PCas (Fig. 1A). ADRB2 was positively correlated with AR staining intensity (Kendall's Tau-b correlation 0.30, $P = 0.011$) and inversely correlated with Gleason Grade in the spot (Kendall's tau-b correlation -0.49, $P < 0.0001$; Fig. 1B). Baseline patient characteristics are shown in Supplementary Table 1. Clinical follow-up data from this cohort showed that patients with low ADRB2 staining intensities had a higher risk of biochemical recurrence than patients with high ADRB2 (HR 0.51, 95 % CI 0.25-1.04, $P = 0.064$). This was fully explained by Gleason grade in the spots (HR for ADRB2 adjusted for Gleason grade: 1.81, 95 % CI 0.61-5.39, $P = 0.29$). Corroborative of an association with luminal differentiation, ADRB2 mRNA was also highly correlated with NKX3.1, AR, KLK3, KLK4 and HOXB13 mRNAs in hormone-naïve tumors in the MSKCC dataset (35) (Fig. 1C). Similarly, we also observed a positive correlation between ADRB2 and NKX3.1 in radical prostatectomy specimens from the Prostate Biobank at the Oslo University Hospital (n=20, Spearman's *rho* = 0.64, $P < 0.01$; Supplementary Fig. S1).

ADRB2 is functionally involved in NEtD of prostate cancer cell lines

Epigenetic silencing of ADRB2 is associated with progressive differentiation of embryonic stem cells towards terminally differentiated neural cells (36), and ADRB2 was recently reported to be among the top downregulated genes in a meta analysis-developed NEPC gene signature (37). However, the direct involvement of ADRB2 in NEPC development has not been investigated. To test the implication of ADRB2 downregulation in a hormone-sensitive adenocarcinoma model system, we employed LNCaP cell line derivatives stably transfected with three different shRNAs targeting ADRB2 mRNA (shADRB2-1, shADRB2-2, shADRB2-3) and a negative control shRNA (shCtrl) (21). shADRB2-1, -2 and -3 presented about 50 %, 85 % and 80 % lowered β-adrenergic receptor ligand binding activity,

respectively, compared to shCtrl, which was also apparent by immunohistochemical staining of formalin-fixed cells (Supplementary Fig. S2A-B).

Microarray expression analysis of shADRB2-2 and shADRB2-3 against shCtrl treated cells revealed 51 commonly differentially expressed genes (DEGs; FDR < 0.05). Pathway enrichment analysis of these genes showed “neuron differentiation” and “neuron projection development” as among the top enriched pathways (Fig. 2A). Using semi-quantitative Real-Time RT-PCR (sqRT-PCR), we validated the decreased expression of four out of five genes implicated in neuron differentiation upon knockdown of ADRB2: Signal transducer CD24 (CD24), SLIT and NTRK Like family member 3 (SLITRK3), jagged canonical Notch ligand 1 (JAG1) and kelch like family member 1 (KLHL1) (Supplementary Fig. S2C). Downregulation of JAG1, and ENO2, to a lesser extent, were also confirmed at the protein level (Supplementary Fig. S2D).

Previous studies on the β-adrenergic signaling pathway (18, 19), and our gene expression analysis on shADRB2 cells suggested a role of ADRB2 in NEtD. Therefore, we hypothesized that lowered expression of neuron differentiation genes in shADRB2 cells would result in impeded NEtD. To this end, we incubated shCtrl and shADRB2 androgen sensitive LNCaP cells in androgen-depleted medium, thus mimicking androgen deprivation therapy. After five days, both transcript and protein levels of the neuronal markers enolase 2 (ENO2) and tubulin beta-3 chain (TUBB3) were lower in shADRB2 than shCtrl cells (Fig. 2B-C). ENO2 and TUBB3 mRNA levels were induced in response to androgen deprivation, as expected, but the effect was less prominent in shADRB2 cells than shCtrl cells (Fig. 2D). In the presence of higher testosterone levels (10% FCS), ENO2 mRNA and protein levels, but not TUBB3 mRNA, were lower in shADRB2 cells than shCtrl cells (Supplementary Fig. S2D-E), suggesting that ENO2 is under control of ADRB2 independently of the androgen levels to which the cells are exposed**.**

In agreement with previous reports on the LNCaP cell line model (38, 39), LNCaP shCtrl cells progressively developed complex cell protrusion networks reminiscent of neurite outgrowths and smaller and more compact soma following androgen depletion (Fig. 2E). After 72 hours androgen depletion, the length of neurites per cell was significantly (t-test all $P < 0.001$) lower in shADRB2 cells compared to shCtrl cells (Fig. 2F). These findings were corroborated by quantification of neurite lengths in independent experiments (n=3) where the cells were incubated in androgen-depleted medium for five days (Fig. 2G). Interestingly, the moderately ADRB2-depleted shADRB2-1 cells only showed a trend towards shorter neurite lengths after five days androgen withdrawal ($P>0.05$), suggesting ADRB2 dosage-dependency. Similar results were obtained after 48 hours of androgen depletion (Supplementary Fig. S2F). Moreover, the average number of branch points per field was also lowered in shADRB2 cells (Fig. 2H).

In line with our previous findings (21), LNCaP shADRB2 cells were less sensitive to anti-androgen treatment than shCtrl cells (Supplementary Fig. S3). These data indicated that, upon challenge with androgen depletion, LNCaP shADRB2 cells had reduced capabilities towards undergoing NEtD. Moreover, these cells were more resistant to treatments targeting the androgen signaling axis than high ADRB2-expressing cells, supporting that shADRB2 cells represent an adeno-CRPC model.

The well known NEtD-promoting effect of β-adrenergic receptor stimulation made us hypothesize that ADRB2 knockdown would abate agonist-induced NEtD under androgen-proficient conditions. After short exposure to the β-adrenergic receptor agonist isoproterenol in androgen-proficient medium, shCtrl and shADRB2-1 developed long and complex neurite outgrowths, whereas the effect was modest in shADRB2-2 and shADRB2-3 (Fig. 2I and Supplementary Fig. S2G), in line with the latter two cell lines having the lowest ADRB2 protein levels. The effects of isoproterenol were abrogated by co-supplementation with the β-adrenergic antagonist propranolol, suggesting the effects were specific. Interestingly, in vehicle-treated cells, shADRB2-2 ($P = 0.1$) and shADRB2-3 ($P < 0.05$) tended to have less neurite outgrowth than shCtrl and shADRB2-1. Interestingly, forskolin (FSK), activating adenylyl cyclase (AC) downstream of ADRB2, rescued neurite outgrowth in the shADRB2 cells, yielding similar neurite lengths per cell as stimulated shCtrl cells (Fig. 2H and Supplementary Fig. S2G).

The observation that shADRB2 cells were capable of transdifferentiating upon cAMP elevation (bypassing ADRB2) suggested that ADRB2 overexpression in shADRB2 cells would mimic this effect and induce NEtD. Indeed, the three shADRB2 cell lines transiently overexpressing ADRB2 developed extensive neurite outgrowth in androgen-proficient medium (Fig. 3A and Supplementary Fig. S4A). We quantified neurite outgrowth and found that it was elevated in all the ADRB2-overexpressing cells compared to pEmpty-transfected cells (Fig. 3B). Total neurite length per cell were similar in ADRB2-overexpressing shCtrl and shADRB2 cells (t-test all $P > 0.05$), and neurite lengths per cell were not different from those developed upon short-term FSK treatment (t-test all $P > 0.10$). We could confirm expression and plasma-membrane localization of ADRB2 using an anti-Flag tag antibody (Supplementary Fig. S4B), and overexpression by radioligand binding assay (data not shown). Surprisingly, transient ADRB2 overexpression did not increase immunofluorescent intensities of TUBB3 although it was present in neurites (Supplementary Fig. S4C). Moreover, both mRNA and protein levels of TUBB3 and other NE markers such as synaptophysin (SYP) and chromogranin A (CHGA) were unchanged following ADRB2 overexpression (data not shown).

To further substantiate the finding that ectopic ADRB2 overexpression induced NE-like morphological characteristics in LNCaP cells, we overexpressed ADRB2 in VCaP and PC-3 cells, both expressing lower ADRB2 protein (Fig. 3C) and mRNA (Fig. 3D) levels than parental LNCaP cells.

Consistent with our results in LNCaP cells, ADRB2 overexpression increased neurite outgrowth also in a subset of VCaP and PC-3 cells (Supplementary Fig. S4D). In both VCaP and PC-3 cells, ADRB2 overexpression led to a higher proportion of cells with neurite outgrowths, particularly in VCaP cells (Fig. 3E). The increase in neurite length was particularly clear and significant in PC-3 cells (Fig. 3F). The NEtD-like morphological changes in PC-3 and VCaP cells upon overexpression of ADRB2 were accompanied by unchanged levels of the NE-markers TUBB3 (Supplementary Fig. S4C), CHGA and SYP, in line with what was observed in LNCaP cells.

Collectively, these data show that ADRB2 promotes neurite outgrowth but not induction of NE markers, whereas ADRB2 depletion abrogates both neurite outgrowth and NE-marker elevation.

Depletion of ADRB2 increases β-catenin activity, and inhibition of GSK3β reduces NE characteristics

The canonical Wnt pathway is believed to be a central factor in the development of CRPC through interaction with AR (40). Moreover, canonical Wnt signaling has been shown to be elevated in neuroendocrine transdifferentiated LNCaP cells and in NE tumors from TRAMP mice (41). We sought to investigate whether stable ADRB2 knockdown could impact this pathway and thereby reduce NEtD in these cells. Western blotting of nuclear cell extracts from shADRB2 LNCaP cells revealed elevated levels of active β-catenin (unphosphorylated at S37 and T41; Fig. 4A). Using a luciferase reporter system, we found that, as expected, androgen depletion led to an elevated TCF/LEF (transcription factors activated by nuclear β-catenin) transcriptional activity which was significantly higher in shADRB2 treated cells, particularly in androgen-depleted medium (Fig. 4B). Re-introduction of ADRB2 in the shADRB2–treated cells tended to decrease the TCF/LEF activity in shADRB2-2 (paired t-test $P = 0.18$) (Fig. 4C). VCaP cells which express lower ADRB2 than LNCaP, showed a higher ratio of active β-catenin to total β-catenin and had higher TCF/LEF reporter activity than LNCaP cells (Supplementary Fig. S5A-B).

We tested whether siRNA-mediated knockdown of β-catenin or direct β-catenin inhibition by supplementation with MSAB would rescue NEtD in shADRB2 cells, and found no effect on NEtD morphology or NE-marker expression (not shown). Activation of β-catenin by GSK3α/β-inhibition with CHIR99021, however, reduced androgen depletion-induced NEtD in shCtrl (Fig. 4D-E). CHIR99021 increased nuclear localization of β-catenin, TCF/LEF reporter activity and total levels of active β-catenin in shCtrl cells (Supplementary Fig. S5C-E). Interestingly, CHIR99021 reduced expression of the neuron differentiation related genes that were downregulated in shADRB2 cells, as well as ENO2 and TUBB3 (Fig. 4F). GSK3α/β regulates multiple signaling pathways aside from the canonical Wnt pathway, and the results collectively suggest that the reduced capability of low-ADRB2 cells to undergo NEtD involves GSK3α/β.

ADRB2 is suppressed in NEPC and associated with NE characteristics

We have previously shown that ADRB2 mRNA is up-regulated in primary prostate cancer and ADT-naïve metastases, and down-regulated following neoadjuvant ADT in primary PCa (24), suggesting an association with disease progression due to the near inevitable emergence of CRPC among these patients. Using multiple publicly available prostate cancer datasets, we confirmed our previous findings that ADRB2 levels were consistently upregulated in primary PCa and elevated in metastases from ADT-naïve patients compared to benign tissue samples (Fig. 5A and Supplementary Fig. S6A). Moreover, ADRB2 mRNA levels were downregulated in CRPC samples, primarily characterized by reactivation of AR and AR-overexpression, compared to treatment-naïve metastases and primary PCs (Fig. 5A and Supplementary Fig. S6A-C).

It has been shown that at least a subset of NEPCs are clonally derived from adeno-CRPCs, and NEPC tumors express low levels of prostate luminal genes (4). Accordingly, in metastatic CRPC samples with NEPC histology, ADRB2 levels were further significantly downregulated compared to adeno-CRPC samples (Fig. 5B). This finding led us to perform a correlative analysis between ADRB2 expression levels with a panel of genes previously shown to be altered in NEPC (Fig. 5C). The gene panel consisted of previously published NEPC/small cell phenotype-associated genes (4, 37) and genes coding for NE markers used in pathological assessment of NEtD/NEPC. Notably, the NEPC WCM cohort showed that the majority (13/16) of metastases with low ADRB2 expression (lower tertile) had histologically confirmed NEPC. Low ADRB2 expression was associated with elevated expression of NE-markers and inversely associated with prostatic luminal markers. Similar associations were found in the FHCRC and SU2C/PCF 2019 cohorts by hierarchical clustering (Supplementary Fig. S6D). Collectively these data corroborate the functional studies presented in this work, namely that loss or lowered ADRB2 expression is a characteristic of, and may be involved in, NEPC development through enabling ADT-induced NEtD.

To understand the molecular downstream effect of ADRB2 activity, we selected the top 400 genes showing positive or negative correlation with ADRB2 expression (800 genes in total) in the NEPC WCM, SU2C/PCF 2015 and FHCRC mCRPC datasets. We then performed an explorative gene ontology analyses on the 400 top genes negatively correlated with ADRB2 in each dataset individually, and 13 enriched pathways were found to overlap between the datasets (Supplementary Fig. S6E). Interestingly, these pathways included generation of neurons (GO:0048699), nervous system development (GO:0007399) and cell differentiation (GO:0030154).

A total of 23 ADRB2-correlated genes were found to overlap between all the datasets. Within these 23 genes we identified 15 genes (Supplementary Table 2) that showed expression levels associated with NEPC histology in the NEPC WCM dataset. Hierarchical clustering revealed that genes

negatively correlated with ADRB2 clustered with NE-up genes, whilst genes positively correlated with ADRB2 expression clustered with high expression of luminal genes (Fig. 5D). Several of the identified genes correlating with ADRB2 have previously been included in NEPC gene signatures (4, 37).

Guided by the hierarchical clustering, we applied the 15 ADRB2-correlated genes and ADRB2 as a t-NEPC gene expression signature (ADRB2 signature). We found that the ADRB2 signature genes were capable to cluster LTL PDX models with an NEPC histology (Fig. 5E; (16)). ADRB2 signature scores were higher among PDXs with an NEPC histology (median Z-score sums of 0.295 and -17.8 for NEPCs and adenocarcinomas, respectively; Wilcoxon rank sum test $P < 0.0001$). By *in silico* reanalysis of longitudinal samples from the LTL331 xenograft, which develops t-NEPC following castration (GSE59984; (42)), ADRB2 mRNA was downregulated upon relapse, and essentially lost after NEPC emergence, alongside loss of luminal markers, elevation of NE-markers, and increased ADRB2 signature scores (Supplementary Fig. S7A). Collectively, these results suggests a utility of the ADRB2 signature as a transcriptomic signature for t-NEPC

To elucidate mechanisms responsible for the observed downregulation of ADRB2 following therapy resistance, we performed a re-analysis of the NEPC WCM cohort for *ADRB2* copy number variation, but found no differences in frequencies of amplifications (20 vs. 22 %) or shallow deletions (3 vs. 7 %) in adeno-CRPCs and NEPCs (χ^2 test, both $P > 0.05$; Supplementary Fig. S7B). These data suggested the ADRB2 is epigenetically or transcriptionally silenced, or destabilized at the mRNA level in NEPC. ADRB2 has been identified as an EZH2 target gene (43) and we observed that EZH2 was inversely correlated with ADRB2 mRNA levels in t-NEPCs but not adeno-CRPCs in the NEPC WCM dataset (Supplementary Fig. S7C). Accordingly, a reanalysis of the GSE107782 dataset (44) showed that both EZH2 inhibition and transient EZH2 knockdown led to modest increases in ADRB2 mRNA levels (Supplementary Fig. S7D). Furthermore, we have previously shown that ADRB2 is highly downregulated in LNCaP cells following androgen depletion (24), and as in LNCaP, a reanalysis of transcriptome data of the LuCaP35 PDX (GSE33316 (45)) showed ADRB2 downregulation following castration (Supplementary Fig. S7E). Likewise, ENZ-challenged CWR-R1, LAPC and LNCaP cells (GSE78201 (46)) showed reduced ADRB2 mRNA levels, with further downregulation of ADRB2 upon acquisition of ENZ resistance (Supplementary Fig. S7F). Although these data collectively suggested that transcription of ADRB2 could be androgen dependent, we have previously shown in androgen depleted LNCaP cells, that ADRB2 protein levels are not elevated upon re-stimulation with varying concentrations of R1881 (24). This is supported by gene expression profiling of androgen depletion-challenged LNCaP cells re-introduced to androgen, showing mRNA upregulation of several androgen responsive genes, but not ADRB2 (Supplementary Fig. S7G).

ADRB2 promotes emergence of NE features during ADT in PCa xenografts

As the transcriptomic data presented showed that ADRB2 expression was consistently and progressively downregulated in CRPC and NEPC, we performed a re-analysis of our LNCaP xenograft model which underwent castration treatment (Fig. 6A; (21)). We found that xenografts of shADRB2 LNCaP cells had significantly increased tumor latencies following injection compared to LNCaP shCtrl xenografts (Fig. 6B-C). To corroborate this finding, we performed colony formation assays with shCtrl and shADRB2 LNCaP cells and VCaP cells, which showed consistently lower colony formation capabilities of shADRB2 and VCaP cells in soft-agar compared to shCtrl (Supplementary Fig. S8A-B). Knockdown of ADRB2 had no or a minor negative effect on proliferation (Supplementary Fig. S8C-D), and was thus likely not responsible for the lowered amount of colonies formed in these cells. GSK3β inhibition using CHIR99021, which reduced NEtD, also reduced colony formation in shCtrl, shADRB2 and VCaP cells (Supplementary Fig. S8E), suggesting that GSK3β could be responsible for loss of both anchorage-independent growth and NEtD.

Importantly, immunohistochemical analyses of tumors that had progressed following castration revealed that tumors that expressed high ADRB2 levels at time of injection expressed more TUBB3 than their low-ADRB2 counterparts (t-test P = 0.038; Fig. 6D-E). As expected, loss of ADRB2 expression was observed in all tumors, regardless of pre-castration ADRB2 levels (Fig. 6D). This suggested that downregulation of ADRB2 mRNA in tumors recurring on ADT and/or ARPI results in lowered protein expression. As tissue vascularization was recently reported to increase with NEtD in PCa (47), we also investigated CD31 by IHC. CD31 tended to be higher in xenograft tumors derived from shCtrl than shADRB2 (t-test P = 0.065, Wilcoxon rank sum test P = 0.13; Fig. 6E).

Based on the presented findings, we propose a model (Fig. 6F) in which high-ADRB2 tumor cells undergo NEtD upon ADT and/or ARPI challenge, which may represent an initial step in the manifestation of NEPC. Tumor cells expressing low ADRB2 levels, on the other hand, respond to treatment by retaining luminal differentiation, which upon acquisition of therapy resistance re-engages the AR and/or re-sensitize to castrate androgen levels and thereby promotes adeno-CRPC development.

Discussion

Progression to NEPC is an increasing challenge as more drugs targeting the androgen signaling axis become part of the toolbox for treating PCa patients. In this study, we have shown that ADRB2 is a luminal marker associated with a well differentiated growth pattern in hormone sensitive tumors. ADRB2 expression was progressively downregulated upon treatment-related resistance development, and the level of ADRB2 in hormone-naïve prostate cancer determines whether or not

the cells are able to undergo NEtD upon androgen deprivation both in cell lines and a mouse xenograft model. High-ADRB2 cells had longer neurite outgrowth and higher expression of neuron differentiation and NE genes than low-ADRB2 cells. Overexpression of ADRB2 in low-ADRB2 cells induced growth of neurite protrusions, and ADRB2 expression was associated with low canonical WNT signaling activity.

The clinical appearance of both adeno-CRPC and t-NEPC is associated with loss of differentiation of luminal cell lineages and gain of lineage plasticity, and these characteristics are most pronounced in NEPC. Recently it was reported that men with high grade disease and disproportionally low serum PSA not only have poor outcomes, but also displayed a neuroendocrine/small cell gene signature (48). The finding that ADRB2 expression in advanced PCa correlated with markers of luminal differentiation and inversely correlated with genes typically upregulated in t-NEPC indicates that suppression of ADRB2 is a feature of AR-low/null PCa variants. In fact, a recent transcriptomic meta-analysis driven search for markers associated with NEPC included ADRB2 in its Meta-12 gene signature (37).

Certain primary tumor characteristics are likely to predispose for t-NEPC development (42), and neuronal genes are the most frequently enriched genes in t-NEPC (37). Androgen withdrawal predictably induces NE features in prostate cancer cell lines (38, 39) and patient tumors (49). NE features have been shown to increase with ADT duration (50), and metastatic CRPCs are more likely than not to present at least focal neuroendocrine differentiation (12), supporting the putative successive relationship between NEtD and t-NEPC (51).

Ample evidence that stimulation of ADRB2 and its' downstream signaling factors confers NEtD in androgen-dependent and -independent PCa cells exists (18, 19, 47), and the sympathetic nervous system and the catecholamine signaling axis are increasingly acknowledged as major factors in PCa oncogenesis and progression (52-54). Our findings illustrate that downregulation of ADRB2 not only repressed ADRB agonist-driven NEtD, but also impaired transdifferentiation upon androgen-withdrawal. Although these findings seemingly contradict the clinical data presented, t-NEPC development may be considered a multistep clonal evolution process involving initial growth inhibition and transdifferentiation (NEtD) followed by a ARPI challenge-induced proliferative switch involving e.g. loss of tumor suppressor function (55, 56).

We propose that high-ADRB2 PCa cells are inherently more prone to undergo NEtD upon challenge with ADT, which may represent an initial, essential step in t-NEPC development appended by transcriptional repression of *ADRB2*. In support of this hypothesis, we have shown that a low ADRB2 protein level is associated with rapid adeno-CRPC progression in patients, and that low-ADRB2 LNCaP cells better retain bioavailable androgens (21) and are less sensitive towards antiandrogens. This theoretically renders them more likely to recur as conventional adeno-CRPCs by

reactivating the androgen signaling axis, and not as t-NEPCs. In support of this, our xenograft model showed that although tumoral ADRB2 protein expression was predictably lost in castrated mice, the level of ADRB2 at time of castration was decisive for NE-like lineage commitment during treatment. Moreover, in absence of treatment challenge, both hormone-sensitive and -insensitive ADRB2-overexpressing PCa cells developed a morphology remniscient of neurons. This was surprisingly not accompanied by elevated NE-marker expression. Although this finding may solely represent an *in vitro* phenomenon, ADRB2's role in NEtD may primarily relate to the neural component of neuroendocrine cells, while treatment-related pressure is necessitous to further drive emergence of a true NE phenotype. A paired longitudinal patient biopsy study on tumor tissue sampled prior and after ARPI treatment was published during revision of this manuscript (57), and it will be interesting to retrospectively see whether treatment-naïve tumors with high ADRB2 are more likely to recur as t-NEPC.

The mechanism(s) responsible for downregulation of ADRB2 upon treatment challenge, NEtD and t-NEPC development remain elusive. Nouri and colleagues showed in multiple PCa cell lines that NEtD is likely preceded by a transient neural/neural crest stem-like reprogramming event, and that ADRB2 mRNA was consistently downregulated in four PCa cell lines upon acquisition of this state (58). Likewise, ADRB2 mRNA was downregulated in Enz-challenged and -resistant PCa cell lines. These findings suggest that transcriptional repression of *ADRB2* is prerequisite for repressing luminal characteristics and allowing reprogramming to lineages with less reliance on AR signaling.

Expanding on this notion, we have found that androgen depletion-mediated ADRB2 downregulation, which is recapitulated in tumors from patients who have undergone ADT, is not rescued by androgen re-supplementation. Moreover, expression levels of ADRB2 and AR were correlated in primary, treatment-naïve PCas, whereas CRPCs were characterized by high AR and low ADRB2 mRNA level. This suggests that ADT-induced transcriptional repression of ADRB2 is not primarily androgen dependent, but may involve other epigenetic and/or transcriptional alterations. In advanced PCa, ADRB2 was anti-correlated with enhancer of Zeste homolog 2 (EZH2), which is enriched in t-NEPCs (4). EZH2 has been shown to silence ADRB2 in a polycomb repressive complex 2 (PRC2)-dependent manner (43), and we found that ADRB2 and EZH2 mRNA levels to be inversely correlated in t-NEPCs, but not adeno-CRPCs in the NEPC WCM dataset. Moreover, during revision of this work, androgen depletion was shown to drive NEtD in PCa cells through induction of β-adrenergic signaling and cAMP response element-binding protein (CREB), which in turn enhanced EZH2 activity (47). In another study, however, knockdown of EZH2 and small molecule EZH2 inhibtors in LNCaP and LNCaP C4-2B cells only led to modest increases in ADRB2 expression. More studies are needed to unravel how ADRB2 expression is regulated during PCa progression and therapy resistance development.

β-blockers (β-adrenergic receptor antagonists) were recently shown to induce expression of EZH2 target genes, including ADRB2, and were shown to represent a compelling therapeutic option for NEPCs (47). Our group has previously shown an association between β-blocker use and reduced cancer specific mortality (59), potentially more so in PCa patients undergoing ADT (60). If the pro-survival of β-blockers is elicited directly on the cancer cells rather than the tumor microenvironment, inhibition of NEtD and thereby preventing or delaying therapy resistance can be one of many mechanisms explaining the possible protective effect observed.

We observed that activation of β-catenin abrogated neurite outgrowth and expression of NE markers and neuron differentiation genes. In agreement with literature (41), NEtD was accompanied by a modest increase in canonical Wnt/β-catenin signaling. Our finding that cells with high Wnt/β-catenin activity were restricted from undergoing NEtD is conflicted by studies indicating a NEtD-promoting effect of Wnt/β-catenin activation (41, 61). Regardless, the ramifications of this signaling pathway are likely context-dependent (62). For instance, β-catenin has been shown to promote transcription of AR target genes in PCa cells (62). Low-ADRB2 LNCaP cells are more androgen responsive (21), and the observed elevation of β-catenin activity in these cells may thus limit androgen depletion-induced NEtD through maintaining an AR transcriptional program that promotes luminal differentiation. We propose that β-blockers may have therapeutic potential for patients with metastatic PCa through potentiating AR-targeted therapy regimens by sustaining a therapy-sensitive luminal lineage and thereby preventing t-NEPC emergence. Concomitantly, β-blockers should theoretically lower cAMP-mediated EZH2 activation. As EZH2 inhibition has been shown to re-sensitize PCa tumors in mice harboring functional loss of TP53 and RB1 to androgen withdrawal (56), studies evaluating the efficacy of combining β-blockers with EZH2 inhibitors are prompted.

In conclusion, we have shown that ADRB2 expression is required for androgen depletion-induced neuroendocrine transdifferentiation, a putative precursory stage of t-NEPC development. Moreover, ADRB2 overexpression was associated with acquisition of NE-like morphological characteristics, and high-ADRB2 xenograft tumors developed NEtD to a higher degree than low-ADRB2 tumors, while castration conferred loss of ADRB2 protein expression. Accordingly, development of adeno-CRPC, and in particular t-NEPC, are associated with downregulation of ADRB2. We suggest that androgen receptor-positive prostate adenocarcinoma cells expressing high levels of ADRB2 are prone to develop t-NEPC, whereas low-ADRB2 cells associate with reactivation of the AR signaling axis and are biased towards adeno-CRPC development.

Acknowledgements

We acknowledge the patients and their families for participation in this study. We also acknowledge our colleagues for their contributions of which we are grateful: Kurt A. Krobert and Finn O. Levy (both University of Oslo; UiO) performed the radioligand binding assays. Solveig Pettersen (Oslo University Hospital; OUH) aided in the acquisition of immunofluorescent images. Stein Waagene and Gunhild Mari Mælandsmo (both OUH) facilitated and helped with the xenograft models. Elise Nilsson (Lund University, Malmö, Sweden) stained our tissue TMA, and Agnieszka Krzyzanowska (Lund University, Malmö, Sweden) updated the patients' clinical data. Hong Qu at NORBRAIN Slidescanning (UiO) scanned whole xenograft tumor tissue sections. The study was supported by funding from UiO, OUH and the Norwegian Cancer Society (NCS) (project #163069). PRB has a PhD grant from the South-Eastern Norway Regional Health Authority (grant #2016043). HHG is funded by NCS (project #206202). AU acknowledges grant support from NCS (#198016-2018). KK is supported by the Sigrid Jusélius Foundation and K. Albin Johanssons stiftelse. IGM is supported by the Norwegian Research Council (#230559), the Movember Prostate Cancer UK Centre of Excellence (#CEO13_2-004) and the John Black Charitable Research Foundation.

Bibliography

1. Loriot Y, Eymard JC, Patrikidou A, Ileana E, Massard C, Albiges L, et al: Prior long response to androgen deprivation predicts response to next-generation androgen receptor axis targeted drugs in castration resistant prostate cancer. *Eur J Cancer* **2015**; 51:1946-1952.
2. Nevedomskaya E, Baumgart SJ, Haendler B: Recent Advances in Prostate Cancer Treatment and Drug Discovery. *Int J Mol Sci* **2018**; 19.
3. Bluemn EG, Coleman IM, Lucas JM, Coleman RT, Hernandez-Lopez S, Tharakan R, et al: Androgen Receptor Pathway-Independent Prostate Cancer Is Sustained through FGF Signaling. *Cancer Cell* **2017**; 32:474-489 e476.
4. Beltran H, Prandi D, Mosquera JM, Benelli M, Puca L, Cyrta J, et al: Divergent clonal evolution of castration-resistant neuroendocrine prostate cancer. *Nat Med* **2016**; 22:298-305.
5. Akamatsu S, Inoue T, Ogawa O, Gleave ME: Clinical and molecular features of treatment-related neuroendocrine prostate cancer. *Int J Urol* **2018**; 25:345-351.
6. Aggarwal R, Huang J, Alumkal JJ, Zhang L, Feng FY, Thomas GV, et al: Clinical and Genomic Characterization of Treatment-Emergent Small-Cell Neuroendocrine Prostate Cancer: A Multi-institutional Prospective Study. *J Clin Oncol* **2018**; 36:2492-2503.
7. Ellis L: Understanding cancer lineage plasticity: reversing therapeutic resistance in metastatic prostate cancer. *Pharmacogenomics* **2017**; 18:597-600.
8. Beltran H, Tagawa ST, Park K, MacDonald T, Milowsky MI, Mosquera JM, et al: Challenges in recognizing treatment-related neuroendocrine prostate cancer. *J Clin Oncol* **2012**; 30:e386-389.
9. Ellis L, Loda M: LSD1: A single target to combat lineage plasticity in lethal prostate cancer. *Proc Natl Acad Sci U S A* **2018**; 115:4530-4531.
10. Aparicio A, Logothetis CJ, Maity SN: Understanding the lethal variant of prostate cancer: power of examining extremes. *Cancer Discov* **2011**; 1:466-468.

11. Small EJ, Huang J, Youngren J, Sokolov A, Aggarwal RR, Thomas G, et al: Characterization of neuroendocrine prostate cancer (NEPC) in patients with metastatic castration resistant prostate cancer (mCRPC) resistant to abiraterone (Abi) or enzalutamide (Enz): Preliminary results from the SU2C/PCF/AACR West Coast Prostate Cancer Dream Team (WCDT). *Journal of Clinical Oncology* **2015**; 33:5003-5003.
12. Sainio M, Visakorpi T, Tolonen T, Ilvesaro J, Bova GS: Expression of neuroendocrine differentiation markers in lethal metastatic castration-resistant prostate cancer. *Pathol Res Pract* **2018**; 214:848-856.
13. Fine SW: Neuroendocrine tumors of the prostate. *Mod Pathol* **2018**; 31:S122-132.
14. Grigore AD, Ben-Jacob E, Farach-Carson MC: Prostate cancer and neuroendocrine differentiation: more neuronal, less endocrine? *Front Oncol* **2015**; 5:37.
15. Zou M, Toivanen R, Mitrofanova A, Floch N, Hayati S, Sun Y, et al: Transdifferentiation as a Mechanism of Treatment Resistance in a Mouse Model of Castration-Resistant Prostate Cancer. *Cancer Discov* **2017**; 7:736-749.
16. Lin D, Wyatt AW, Xue H, Wang Y, Dong X, Haegert A, et al: High fidelity patient-derived xenografts for accelerating prostate cancer discovery and drug development. *Cancer Res* **2014**; 74:1272-1283.
17. Lotan TL, Gupta NS, Wang W, Toubaji A, Haffner MC, Chaux A, et al: ERG gene rearrangements are common in prostatic small cell carcinomas. *Mod Pathol* **2011**; 24:820-828.
18. Delgado-González E, Sánchez-Tusie AA, Morales G, Aceves C, Anguiano B: Triiodothyronine Attenuates Prostate Cancer Progression Mediated by β-Adrenergic Stimulation. *Molecular Medicine* **2016**; 22:1-11.
19. Cox ME, Deeble PD, Lakhani S, Parsons SJ: Acquisition of neuroendocrine characteristics by prostate tumor cells is reversible: implications for prostate cancer progression. *Cancer Res* **1999**; 59:3821-3830.
20. Tassidis H, Brokken LJ, Jirstrom K, Ehrnstrom R, Ponten F, Ulmert D, et al: Immunohistochemical detection of tyrosine phosphatase SHP-1 predicts outcome after radical prostatectomy for localized prostate cancer. *Int J Cancer* **2010**; 126:2296-2307.
21. Braadland PR, Grytli HH, Ramberg H, Katz B, Kellman R, Gauthier-Landry L, et al: Low beta(2)-adrenergic receptor level may promote development of castration resistant prostate cancer and altered steroid metabolism. *Oncotarget* **2016**; 7:1878-1894.
22. Edgar R, Domrachev M, Lash AE: Gene Expression Omnibus: NCBI gene expression and hybridization array data repository. *Nucleic Acids Res* **2002**; 30:207-210.
23. Krobert KA, Bach T, Syversveen T, Kvingedal AM, Levy FO: The cloned human 5-HT7 receptor splice variants: a comparative characterization of their pharmacology, function and distribution. *Naunyn Schmiedebergs Arch Pharmacol* **2001**; 363:620-632.
24. Ramberg H, Eide T, Krobert KA, Levy FO, Dizeyi N, Bjartell AS, et al: Hormonal regulation of beta2-adrenergic receptor level in prostate cancer. *Prostate* **2008**; 68:1133-1142.
25. Fanti Z, De-Miguel FF, Martinez-Perez ME: A method for semiautomatic tracing and morphological measuring of neurite outgrowth from DIC sequences. *Conf Proc IEEE Eng Med Biol Soc* **2008**; 2008:1196-1199.
26. Tang Y, Hu LA, Miller WE, Ringstad N, Hall RA, Pitcher JA, et al: Identification of the endophilins (SH3p4/p8/p13) as novel binding partners for the beta1-adrenergic receptor. *Proc Natl Acad Sci U S A* **1999**; 96:12559-12564.
27. Gao J, Aksoy BA, Dogrusoz U, Dresdner G, Gross B, Sumer SO, et al: Integrative analysis of complex cancer genomics and clinical profiles using the cBioPortal. *Sci Signal* **2013**; 6:pl1.
28. Cerami E, Gao J, Dogrusoz U, Gross BE, Sumer SO, Aksoy BA, et al: The cBio cancer genomics portal: an open platform for exploring multidimensional cancer genomics data. *Cancer Discov* **2012**; 2:401-404.

29. Kumar A, Coleman I, Morrissey C, Zhang X, True LD, Gulati R, et al: Substantial interindividual and limited intraindividual genomic diversity among tumors from men with metastatic prostate cancer. *Nat Med* **2016**; 22:369-378.
30. Robinson D, Van Allen EM, Wu YM, Schultz N, Lonigro RJ, Mosquera JM, et al: Integrative Clinical Genomics of Advanced Prostate Cancer. *Cell* **2015**; 162:454.
31. Abida W, Cyrta J, Heller G, Prandi D, Armenia J, Coleman I, et al: Genomic correlates of clinical outcome in advanced prostate cancer. *Proc Natl Acad Sci U S A* **2019**.
32. Grasso CS, Wu YM, Robinson DR, Cao X, Dhanasekaran SM, Khan AP, et al: The mutational landscape of lethal castration-resistant prostate cancer. *Nature* **2012**; 487:239-243.
33. Prensner JR, Iyer MK, Balbin OA, Dhanasekaran SM, Cao Q, Brenner JC, et al: Transcriptome sequencing across a prostate cancer cohort identifies PCAT-1, an unannotated lincRNA implicated in disease progression. *Nat Biotechnol* **2011**; 29:742-749.
34. Huang da W, Sherman BT, Lempicki RA: Systematic and integrative analysis of large gene lists using DAVID bioinformatics resources. *Nat Protoc* **2009**; 4:44-57.
35. Taylor BS, Schultz N, Hieronymus H, Gopalan A, Xiao Y, Carver BS, et al: Integrative genomic profiling of human prostate cancer. *Cancer Cell* **2010**; 18:11-22.
36. Mohn F, Weber M, Rebhan M, Roloff TC, Richter J, Stadler MB, et al: Lineage-specific polycomb targets and de novo DNA methylation define restriction and potential of neuronal progenitors. *Mol Cell* **2008**; 30:755-766.
37. Tsai HK, Lehrer J, Alshalalfa M, Erho N, Davicioni E, Lotan TL: Gene expression signatures of neuroendocrine prostate cancer and primary small cell prostatic carcinoma. *BMC Cancer* **2017**; 17:759.
38. Shen R, Dorai T, Szaboles M, Katz AE, Olsson CA, Buttyan R: Transdifferentiation of cultured human prostate cancer cells to a neuroendocrine cell phenotype in a hormone-depleted medium. *Urol Oncol* **1997**; 3:67-75.
39. Cerasuolo M, Paris D, Iannotti FA, Melck D, Verde R, Mazzarella E, et al: Neuroendocrine Transdifferentiation in Human Prostate Cancer Cells: An Integrated Approach. *Cancer Res* **2015**; 75:2975-2986.
40. Yokoyama NN, Shao S, Hoang BH, Mercola D, Zi X: Wnt signaling in castration-resistant prostate cancer: implications for therapy. *Am J Clin Exp Urol* **2014**; 2:27-44.
41. Ciarlo M, Benelli R, Barbieri O, Minghelli S, Barboro P, Balbi C, et al: Regulation of neuroendocrine differentiation by AKT/hnRNPK/AR/beta-catenin signaling in prostate cancer cells. *Int J Cancer* **2012**; 131:582-590.
42. Akamatsu S, Wyatt AW, Lin D, Lysakowski S, Zhang F, Kim S, et al: The Placental Gene PEG10 Promotes Progression of Neuroendocrine Prostate Cancer. *Cell Rep* **2015**; 12:922-936.
43. Yu J, Cao Q, Mehra R, Laxman B, Yu J, Tomlins SA, et al: Integrative genomics analysis reveals silencing of beta-adrenergic signaling by polycomb in prostate cancer. *Cancer Cell* **2007**; 12:419-431.
44. Kim J, Lee Y, Lu X, Song B, Fong KW, Cao Q, et al: Polycomb- and Methylation-Independent Roles of EZH2 as a Transcription Activator. *Cell Rep* **2018**; 25:2808-2820 e2804.
45. Sun Y, Wang BE, Leong KG, Yue P, Li L, Jhunjhunwala S, et al: Androgen deprivation causes epithelial-mesenchymal transition in the prostate: implications for androgen-deprivation therapy. *Cancer Res* **2012**; 72:527-536.
46. Kregel S, Chen JL, Tom W, Krishnan V, Kach J, Brechka H, et al: Acquired resistance to the second-generation androgen receptor antagonist enzalutamide in castration-resistant prostate cancer. *Oncotarget* **2016**; 7:26259-26274.
47. Zhang Y, Zheng D, Zhou T, Song H, Hulsurkar M, Su N, et al: Androgen deprivation promotes neuroendocrine differentiation and angiogenesis through CREB-EZH2-TSP1 pathway in prostate cancers. *Nat Commun* **2018**; 9:4080.
48. Mahal BA, Yang DD, Wang NQ, Alshalalfa M, Davicioni E, Choeurng V, et al: Clinical and Genomic Characterization of Low-Prostate-specific Antigen, High-grade Prostate Cancer. *Eur Urol* **2018**.

49. Jiborn T, Bjartell A, Abrahamsson PA: Neuroendocrine differentiation in prostatic carcinoma during hormonal treatment. *Urology* **1998**; 51:585-589.
50. Hirano D, Okada Y, Minei S, Takimoto Y, Nemoto N: Neuroendocrine differentiation in hormone refractory prostate cancer following androgen deprivation therapy. *Eur Urol* **2004**; 45:586-592; discussion 592.
51. Parimi V, Goyal R, Poropatich K, Yang XJ: Neuroendocrine differentiation of prostate cancer: a review. *Am J Clin Exp Urol* **2014**; 2:273-285.
52. Hassan S, Karpova Y, Baiz D, Yancey D, Pullikuth A, Flores A, et al: Behavioral stress accelerates prostate cancer development in mice. *J Clin Invest* **2013**; 123:874-886.
53. Magnon C, Hall SJ, Lin J, Xue X, Gerber L, Freedland SJ, et al: Autonomic nerve development contributes to prostate cancer progression. *Science* **2013**; 341:1236361.
54. Zahalka AH, Arnal-Estape A, Maryanovich M, Nakahara F, Cruz CD, Finley LWS, et al: Adrenergic nerves activate an angio-metabolic switch in prostate cancer. *Science* **2017**; 358:321-326.
55. Mu P, Zhang Z, Benelli M, Karthaus WR, Hoover E, Chen CC, et al: SOX2 promotes lineage plasticity and antiandrogen resistance in TP53- and RB1-deficient prostate cancer. *Science* **2017**; 355:84-88.
56. Ku SY, Rosario S, Wang Y, Mu P, Seshadri M, Goodrich ZW, et al: Rb1 and Trp53 cooperate to suppress prostate cancer lineage plasticity, metastasis, and antiandrogen resistance. *Science* **2017**; 355:78-83.
57. Aggarwal RR, Quigley DA, Huang J, Zhang L, Beer TM, Rettig MB, et al: Whole Genome and Transcriptional Analysis of Treatment-Emergent Small Cell Neuroendocrine Prostate Cancer Demonstrates Intra-Class Heterogeneity. *Mol Cancer Res* **2019**.
58. Nouri M, Caradec J, Lubik AA, Li N, Hollier BG, Takhar M, et al: Therapy-induced developmental reprogramming of prostate cancer cells and acquired therapy resistance. *Oncotarget* **2017**; 8:18949-18967.
59. Grytli HH, Fagerland MW, Fossa SD, Tasken KA: Association between use of beta-blockers and prostate cancer-specific survival: a cohort study of 3561 prostate cancer patients with high-risk or metastatic disease. *Eur Urol* **2014**; 65:635-641.
60. Grytli HH, Fagerland MW, Fossa SD, Tasken KA, Haheim LL: Use of beta-blockers is associated with prostate cancer-specific survival in prostate cancer patients on androgen deprivation therapy. *Prostate* **2013**; 73:250-260.
61. Yang X, Chen MW, Terry S, Vacherot F, Chopin DK, Bemis DL, et al: A human- and male-specific protocadherin that acts through the wnt signaling pathway to induce neuroendocrine transdifferentiation of prostate cancer cells. *Cancer Res* **2005**; 65:5263-5271.
62. Pakula H, Xiang D, Li Z: A Tale of Two Signals: AR and WNT in Development and Tumorigenesis of Prostate and Mammary Gland. *Cancers (Basel)* **2017**; 9.

Figure legends

Fig. 1. ADRB2 associates with luminal differentiation. A, Representative images from TMA cores of prostate adenocarcinomas with GG 2, 3 and 4 after immunohistochemical staining with an ADRB2 antibody. **B**, Distributions of ADRB2 staining intensities within each Gleason grade (76 pairs) and AR staining intensities (71 pairs). **C**, ADRB2 mRNA level is plotted against mRNA levels of luminal differentiation markers in primary, untreated tumors in the MSKCC 2010 dataset. Spearman's correlations (rho) are shown for each gene pair with corresponding significance levels.

Fig. 2. ADRB2 is functionally involved in androgen depletion- and β-adrenergic signaling pathway mediated NEtD. A, Venn diagram of genes differentially expressed in shADRB2-2 and shADRB2-3, both compared to shCtrl (FDR < 0.05). The top five enriched pathways identified by DAVID v6.7 are shown, with differentially expressed genes involved in neuron differentiation indicated on the right. **B**, ENO2 and TUBB3 mRNA levels in shADRB2 and shCtrl cells incubated in 2 % CSS for five days were measured using sqRT-PCR. Bars represent mean ADRB2 mRNA levels relative to shCtrl. **C**, Representative Western blots visualizing ENO2 (NSE) and TUBB3 protein levels in whole cell protein extracts from shCtrl and shADRB2 cells incubated in 2 % CSS for five days. **D**, Relative changes in ENO2 and TUBB3 mRNA levels in shCtrl and shADRB2 cells (n=2 for shADRB2-3) after withdrawal of androgens. Expression levels are shown as CSS (5 days) relative to FCS-treated cells. The dotted line indicates 1 (no change in expression). **E**, Representative fields from phase-contrast light microscopy images of LNCaP shCtrl and shADRB2 cultured in 2 % CSS for five days (scale bars = 50 µm). **F**, Neurite lengths were automatically quantified using the IncuCyte S3 Imaging System in six representative fields captured from shCtrl and shADRB2 cells challenged with 2 % CSS for 72 hours. Bars represent mean neurite length related to the cell number per field from ≥3 independent experiments. **G**, In independent biological experiments, neurite lengths were quantified in shCtrl and shADRB2 cells incubated in 2 % CSS 5 days by manual neurite tracing, and bars represent mean field-wise neurite lengths per cell number in each field relative to shCtrl, with ≥2 technical replicates per independent experiment. **H**, The number of branch points in CSS-challenged shCtrl and shADRB2 cells were measured per field and related to the total area. **I**, Mean neurite lengths per cell were manually quantified in fields acquired from cells incubated in androgen-proficient conditions (FCS) with vehicle, or 10 µM of either isoproterenol (ISO), ISO+propranolol (ISO+PRO) or forskolin (FSK) for 90 min. All experiments were performed in ≥3 biological replicates. Statistical significance was tested using two-sided t-tests, and categorized significance levels are indicated by asterisks (*: $P < 0.05$; **: $P<0.01$; ***: $P<0.001$). Error bars indicate SEM.

Fig. 3. Ectopic ADRB2 overexpression induces neurite outgrowth in cell line models with different ADRB2 levels. A, Representative fields from phase-contrast light microscopy images captured from LNCaP shCtrl, shADRB2 and parental LNCaP cells following 48h transfection with pEmpty (pcDNA3.1/Zeo) or pADRB2 (pcDNA3 Flag beta-2-adrenergic-receptor) under androgen-proficient conditions (scale bars = 50 µm). **B**, Neurite lengths per cell in LNCaP shCtrl and shADRB2 cells transfected for 48h with pEmpty- orpADRB2 in androgen proficient medium. **C**, ^{125}I-CYP specific binding to membrane protein fractions from parental LNCaP, VCaP and PC-3 cells was determined. Membrane-bound ADRB2 levels are shown as mean fmol/mg protein in the membrane fractions. **D**, Quantile normalized ADRB2 mRNA levels in LNCaP, VCaP and PC-3 cells accessible from GSE25183. **E**, Fraction of cells displaying neurite outgrowth in VCaP and PC-3 cells transfected with pEmpty or pADRB2 for 48h in androgen-proficient medium. **F**, Neurite length per cell in pADRB2-transfected PC-3 cells relative to pEmpty-transfected cells. All experiments were performed in ≥3 biological replicates. Statistical significance was tested using two-sided t-tests, and categorized significance levels are indicated by asterisks (*: $P < 0.05$; **: $P<0.01$; ***: $P<0.001$). Error bars indicate SEM.

Fig. 4. ADRB2 knockdown increases β-catenin activity, and GSK3β-inhibition reduces NE characteristics. A, Representative Western blot of active β-catenin in nuclear extracts from shCtrl and shADRB2 cells. Histone H3 was used as loading control. **B**, SEAP-normalized TCF/LEF-driven luciferase activities of shCtrl and shADRB2 cells transfected with after incubation in 10 % FCS or 2 % CSS for 48 hours. **C**, SEAP-normalized TCF/LEF activities of shADRB2-2 cells transfected with pEmpty or pADRB2 in androgen-proficient medium. **D**, Representative fields from phase contrast light microscopy-captured images of LNCaP parental cells incubated for 48h in 2 % CSS supplemented with vehicle or 10 µM CHIR99021 (CHIR). **E**, Neurite lengths per cell quantified in fields from cells treated as in (D). **F**, Normalized mRNA levels of neuron differentiation genes differentially expressed in shADRB2 cells (JAG1, SLITRK3, CD24 and KLHL1) and NE-markers ENO2 and TUBB3 in LNCaP parental cells incubated in androgen-proficient medium supplemented with either vehicle or 10 µM CHIR99021 for 24 or 48 hours. mRNA levels were measured using sqRT-PCR, and bars represent expression levels relative to vehicle-treated cells. All experiments were performed in ≥3 biological replicates. Statistical significance was tested using two-sided t-tests, and categorized significance levels are indicated by asterisks (*: $P < 0.05$; **: $P<0.01$; ***: $P<0.001$). Error bars indicate SEM.

Fig. 5. ADRB2 mRNA is downregulated following ADT and CRPC emergence, and further downregulated in t- NEPC. A, Scale-normalized ADRB2 expression in benign, primary PCa, adeno-CRPC and NEPC tissue from the Grasso et al. 2012 (GSE35988) dataset, from each microarray platform individually. **B**, ADRB2 gene expression levels are shown for adeno-CRPC samples, samples

with histologically confirmed NEPC, or samples with NE features in the NEPC WCM, FHCRC and SU2C/PCF 2019 clinical datasets. **C**, Heatmap showing scale-normalized expression of a selection of NE-genes, prostate luminal genes, and a set of genes coordinately correlating with ADRB2 (positively: ADRB2+corr; negatively: ADRB2-corr) in the NEPC WCM, SU2C/PCF and FHCRC datasets is shown. Samples are annotated based on ADRB2 expression level (tertiles; high, intermediate and low) and histological NEPC classification or presence of NE-features. **D**, Gene-wise hierarchical clustering (Ward.D) of the genes used in (C) on the NEPC WCM dataset. **E**, Hierarchical clustering (Ward.D) of mRNA expression levels of ADRB2 and its positively and negatively correlated genes and the LTL PDX models deposited under GSE41193. ADRB2 signature scores for each model are annotated above the heatmap. Statistical significance was tested using Wilcoxon rank sum test, and categorized significance levels are indicated by asterisks (*: $P < 0.05$; **: $P < 0.01$; ****: $P < 0.0001$). NS indicates $P > 0.05$.

Fig. 6. Castration induces NEtD and ADRB2 loss, but a high pre-treatment tumoral ADRB2 level promotes NEtD, in LNCaP xenografts. A, Schematic overview of the used xenograft model. **B**, Tumor growth was monitored weekly by caliper measurements following injection of LNCaP shCtrl (n=30), shADRB2-1 (n=13) and shADRB2-2 (n=15) in NSG mice, and is shown as mean tumor size (mm^2) ± SEM. Statistical significance was tested for tumor volumes at each time-point for each shADRB2 xenograft model relative to shCtrl (Wilcoxon rank sum test). **C**, Boxplot showing the distribution of time from subcutaneous injection to first detection of a palpable tumor for each xenograft model individually. Two mice injected with shADRB2-1 cells did not develop palpable tumors. Statistical significance of differences in time to take relative to shCtrl was calculated by Wilcoxon rank sum test. **D**, Representative light microscopy images of sectioned tumors from two representative mice (#40: shCtrl; #34: shADRB2-2) at termination (post-castration) stained with anti-ADRB2 or anti-TUBB3 antibodies. All tumors lacked expression of ADRB2. The TUBB3-stained sections illustrate areas with the most pronounced staining intensity for the two mice individually. Scale bars = 100 µm. **E**, Whole tumor sections from shCtrl (n=12) and shADRB2-2 (n=10) stained with anti-TUBB3 and anti-CD31 antibodies were analyzed for percentage of positive areas per whole tumor, and are shown as box-and-beeswarm plots. Statistical significance between distributions were calculated using two-sided t-tests. **F**, Proposed model for the divergence in clonal evolution of advanced prostate cancer depending on treatment-naïve ADRB2 levels. Statistical significance was tested by Wilcoxon rank sum tests and is indicated by asterisks (*: $P < 0.05$; **: $P < 0.01$; ***: $P < 0.001$).

Figure 1

A

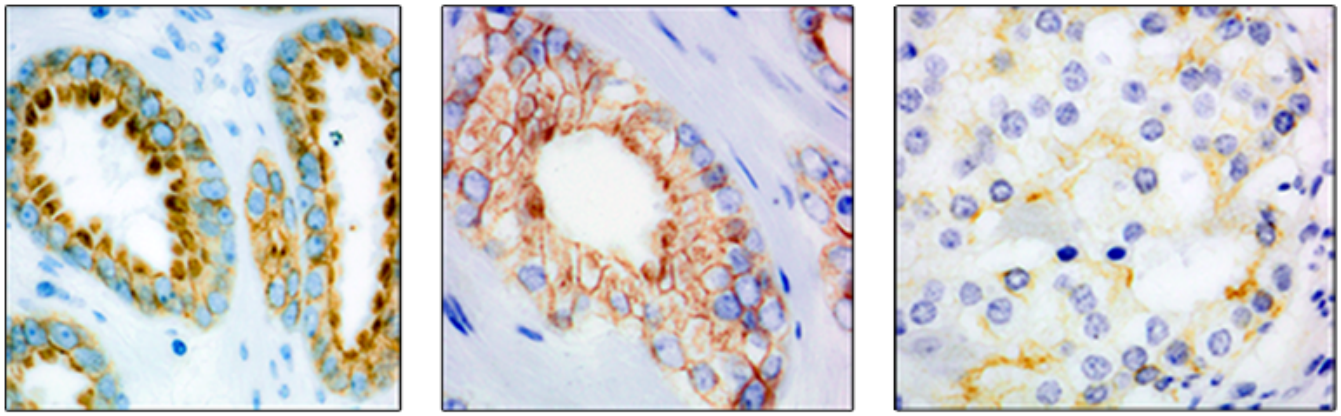
GG2
GG3
GG4

B

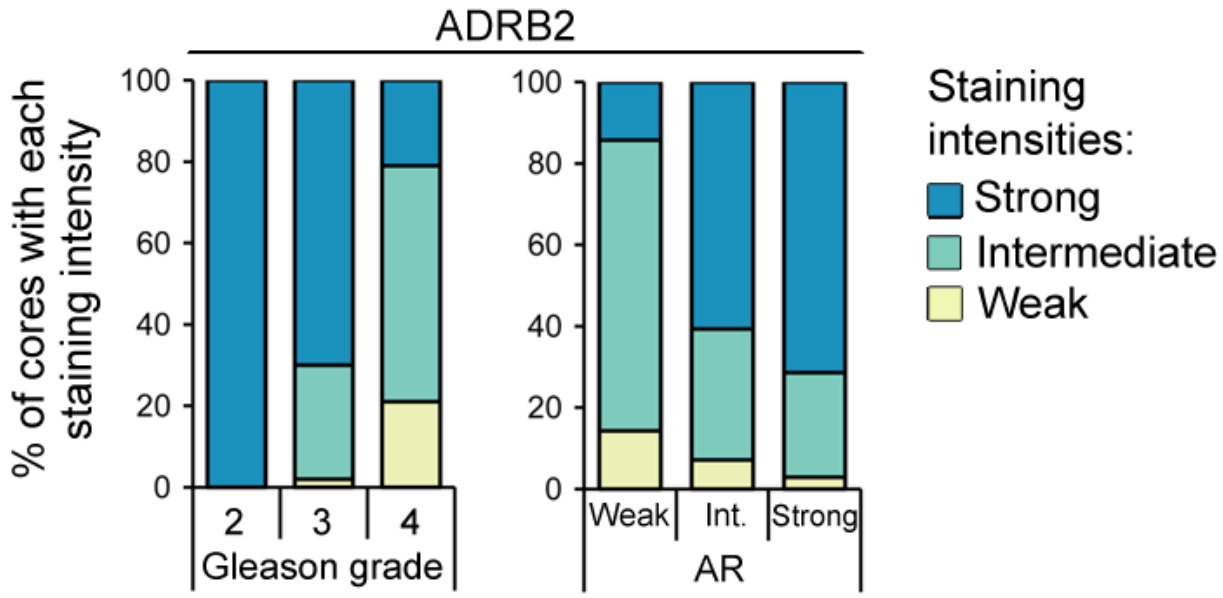
ADRB2
% of cores with each staining intensity
100
80
60
40
20
0
2
3
4
Gleason grade
Weak
Int.
Strong
AR
Staining intensities:
Strong
Intermediate
Weak

C

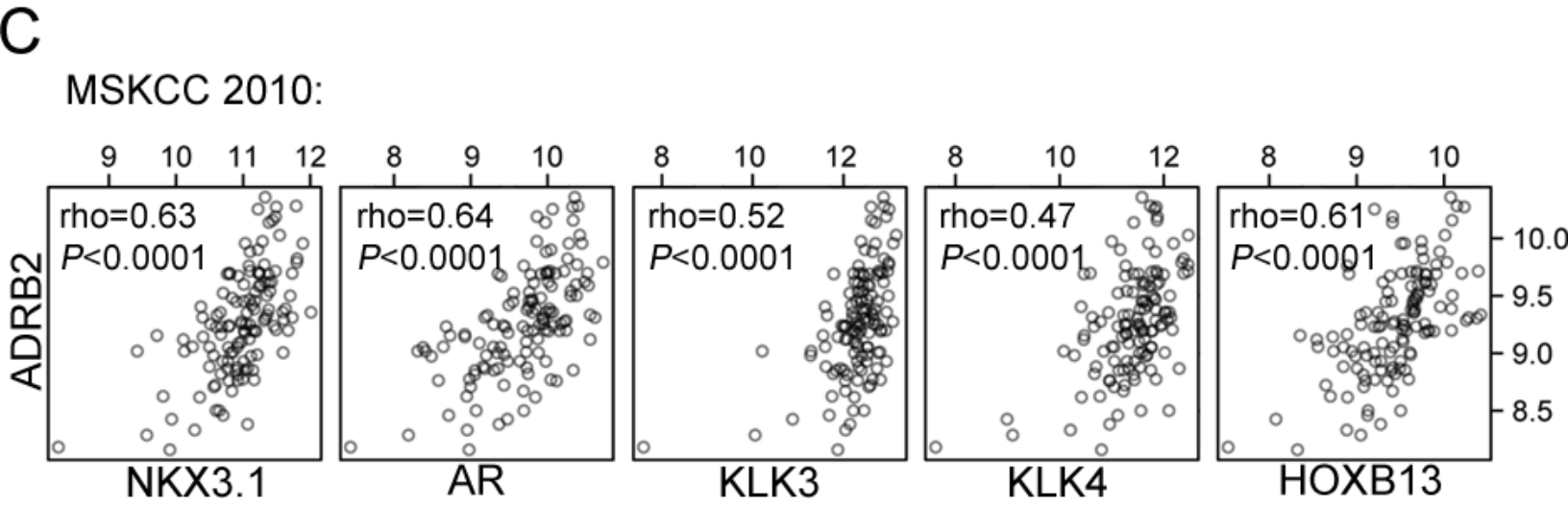
MSKCC 2010:
ADRB2
rho=0.63
P<0.0001
NKX3.1
rho=0.64
P<0.0001
AR
rho=0.52
P<0.0001
KLK3
rho=0.47
P<0.0001
KLK4
rho=0.61
P<0.0001
HOXB13
10.0
9.5
9.0
8.5

Figure 2

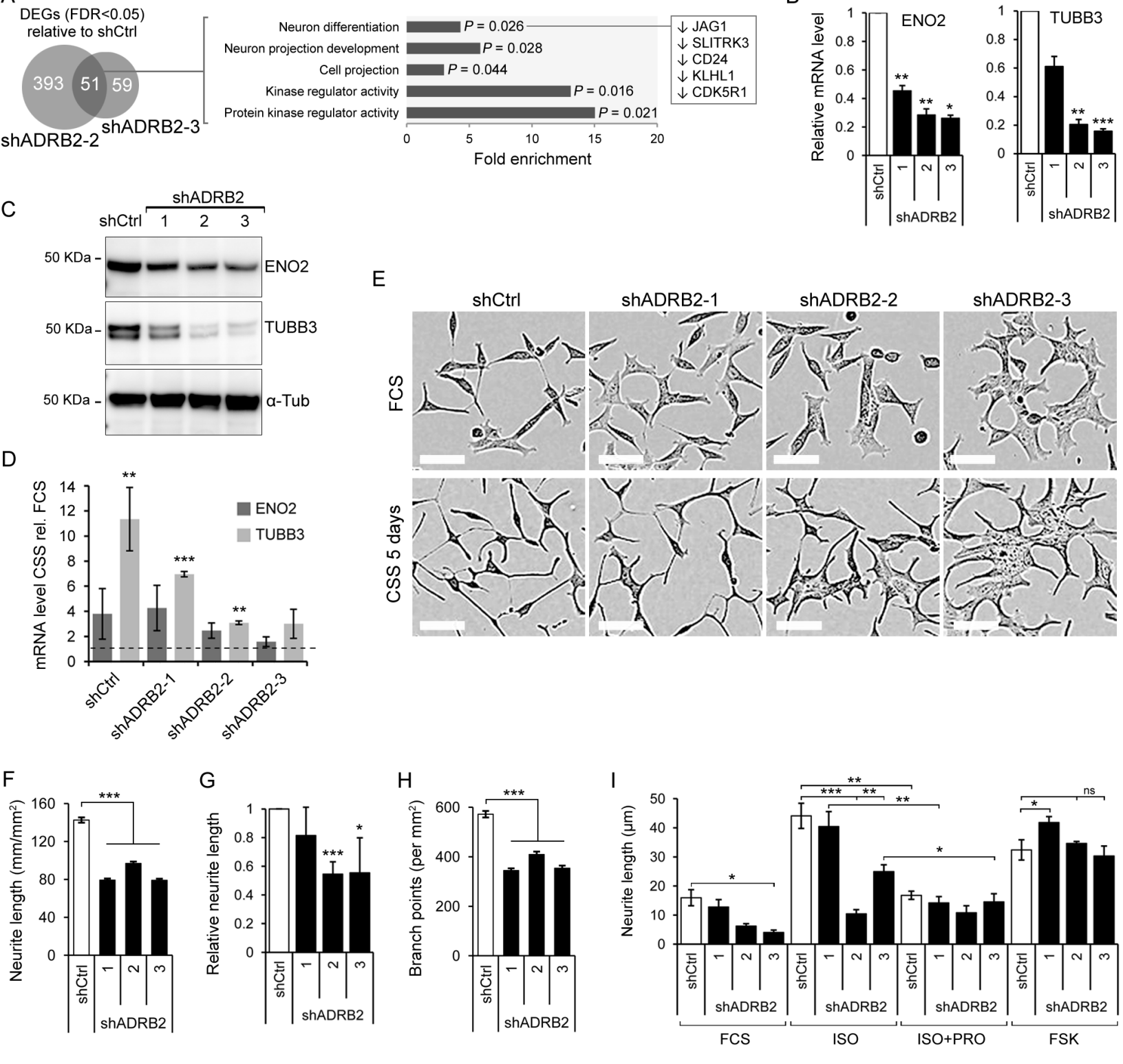
A
DEGs (FDR<0.05)
relative to shCtrl
393
51
59
shADRB2-2
shADRB2-3
Neuron differentiation
Neuron projection development
Cell projection
Kinase regulator activity
Protein kinase regulator activity
P = 0.026
P = 0.028
P = 0.044
P = 0.016
P = 0.021
↓ JAG1
↓ SLITRK3
↓ CD24
↓ KLHL1
↓ CDK5R1
Fold enrichment
B
Relative mRNA level
ENO2
TUBB3
shCtrl
shADRB2
C
shADRB2
shCtrl 1 2 3
50 KDa
ENO2
TUBB3
α-Tub
D
mRNA level CSS rel. FCS
ENO2
TUBB3
shCtrl
shADRB2-1
shADRB2-2
shADRB2-3
E
shCtrl
shADRB2-1
shADRB2-2
shADRB2-3
FCS
CSS 5 days
F
Neurite length (mm/mm²)
G
Relative neurite length
H
Branch points (per mm²)
I
Neurite length (µm)
shADRB2
FCS
ISO
ISO+PRO
FSK
ns

Figure 3

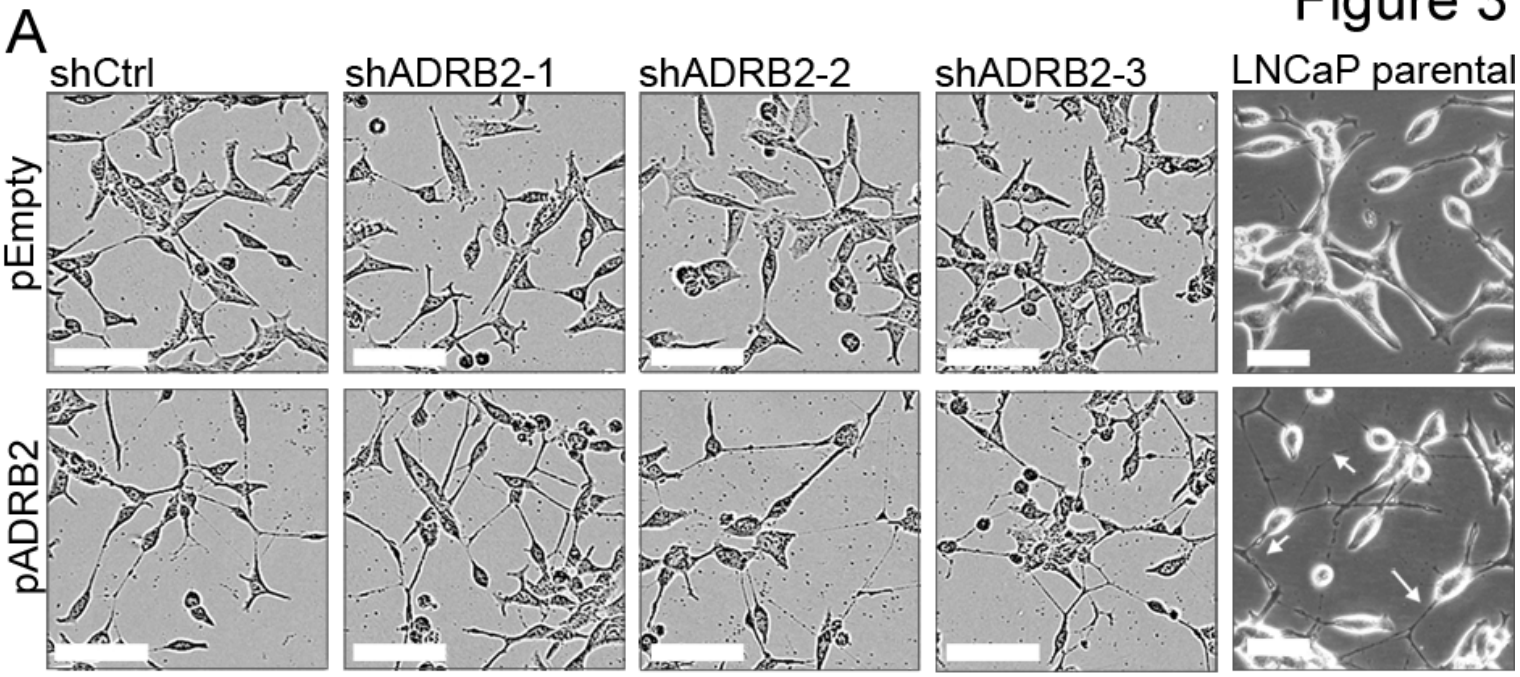
A
shCtrl
shADRB2-1
shADRB2-2
shADRB2-3
LNCaP parental
pEmpty
pADRB2

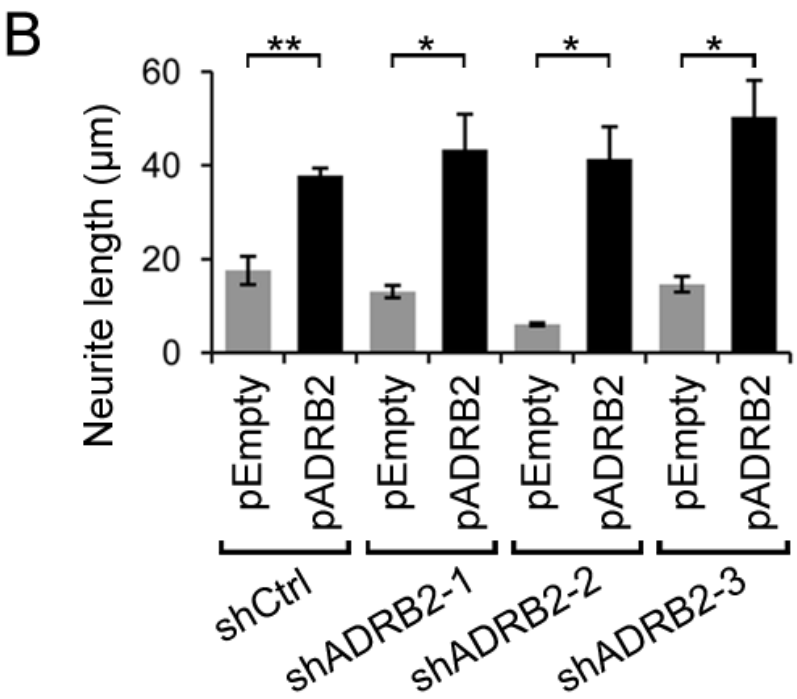
B
Neurite length (μm)
60
40
20
0
**
*
*
*
pEmpty
pADRB2
shCtrl
shADRB2-1
shADRB2-2
shADRB2-3

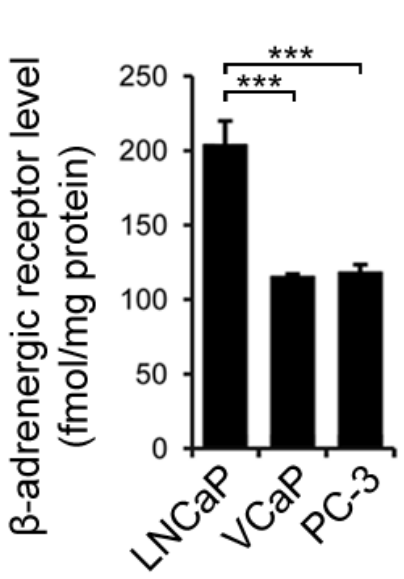
C
β-adrenergic receptor level
(fmol/mg protein)
250
200
150
100
50
0
***
***
LNCaP
VCaP
PC-3

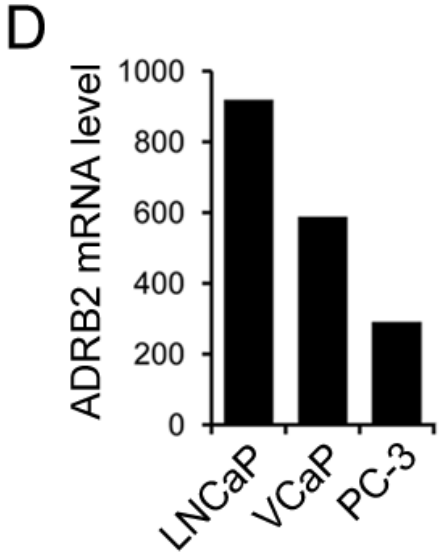
D
ADRB2 mRNA level
1000
800
600
400
200
0
LNCaP
VCaP
PC-3

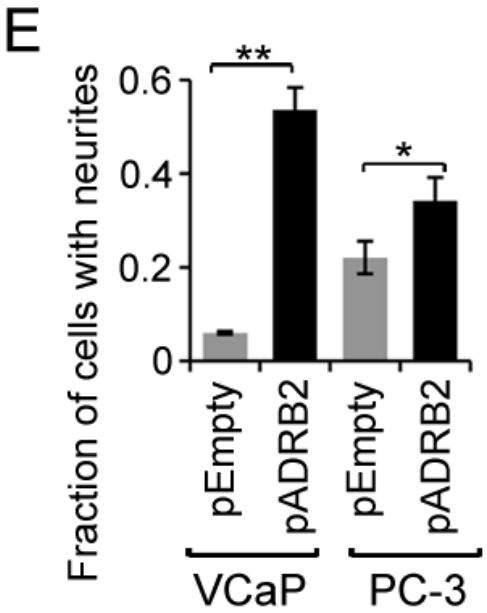
E
Fraction of cells with neurites
0.6
0.4
0.2
0
**
*
pEmpty
pADRB2
VCaP
PC-3

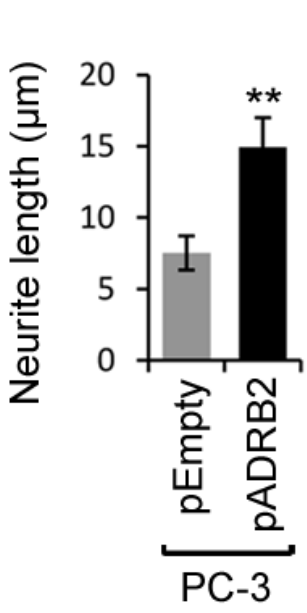
F
Neurite length (μm)
20
15
10
5
0
**
pEmpty
pADRB2
PC-3

Figure 4

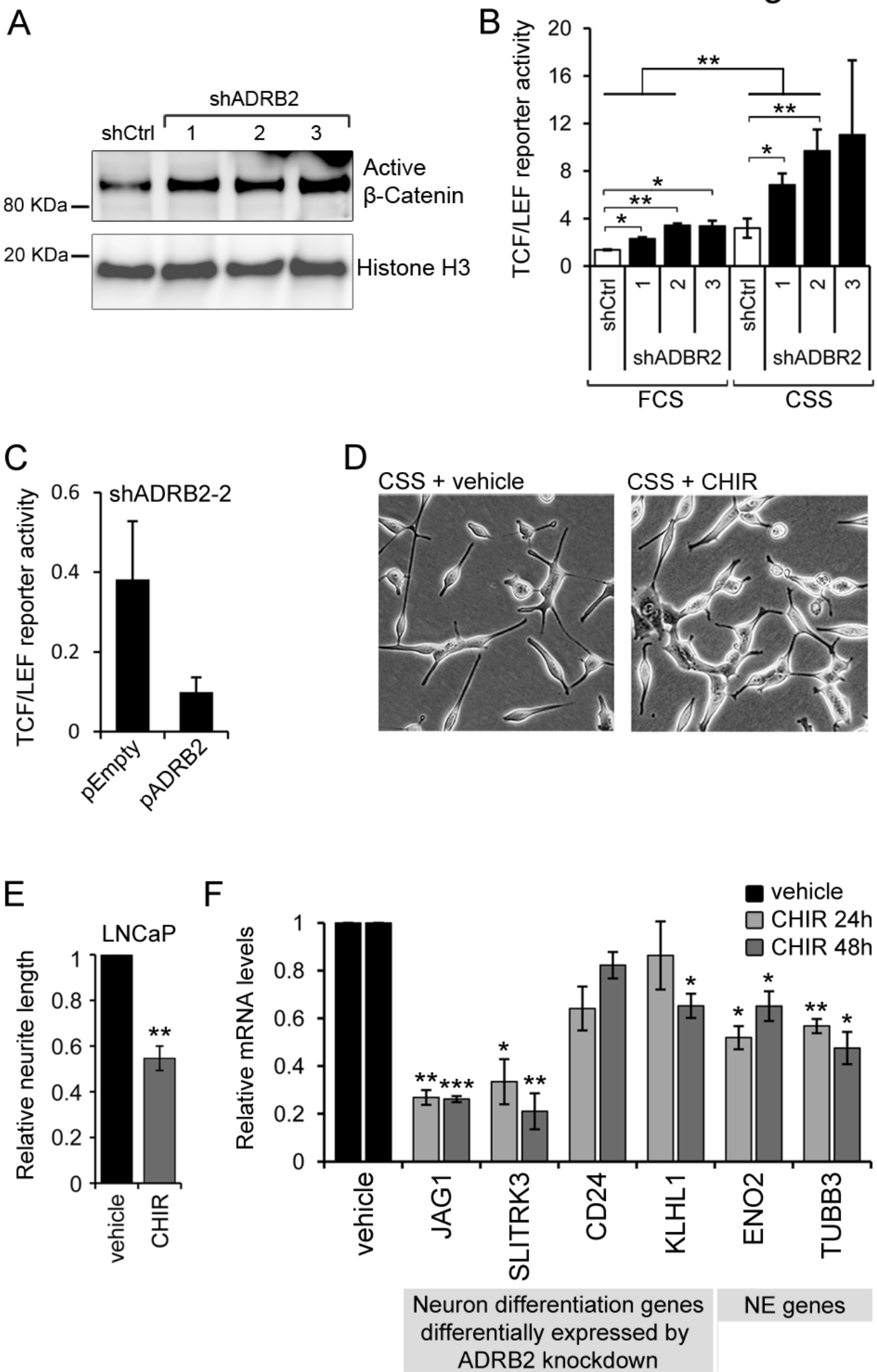
A
shADRB2
shCtrl
1
2
3
80 KDa
Active β-Catenin
20 KDa
Histone H3
B
TCF/LEF reporter activity
shCtrl
shADBR2
FCS
CSS
C
shADRB2-2
TCF/LEF reporter activity
pEmpty
pADRB2
D
CSS + vehicle
CSS + CHIR
E
LNCaP
Relative neurite length
vehicle
CHIR
F
vehicle
CHIR 24h
CHIR 48h
Relative mRNA levels
JAG1
SLITRK3
CD24
KLHL1
ENO2
TUBB3
Neuron differentiation genes differentially expressed by ADRB2 knockdown
NE genes

Figure 5

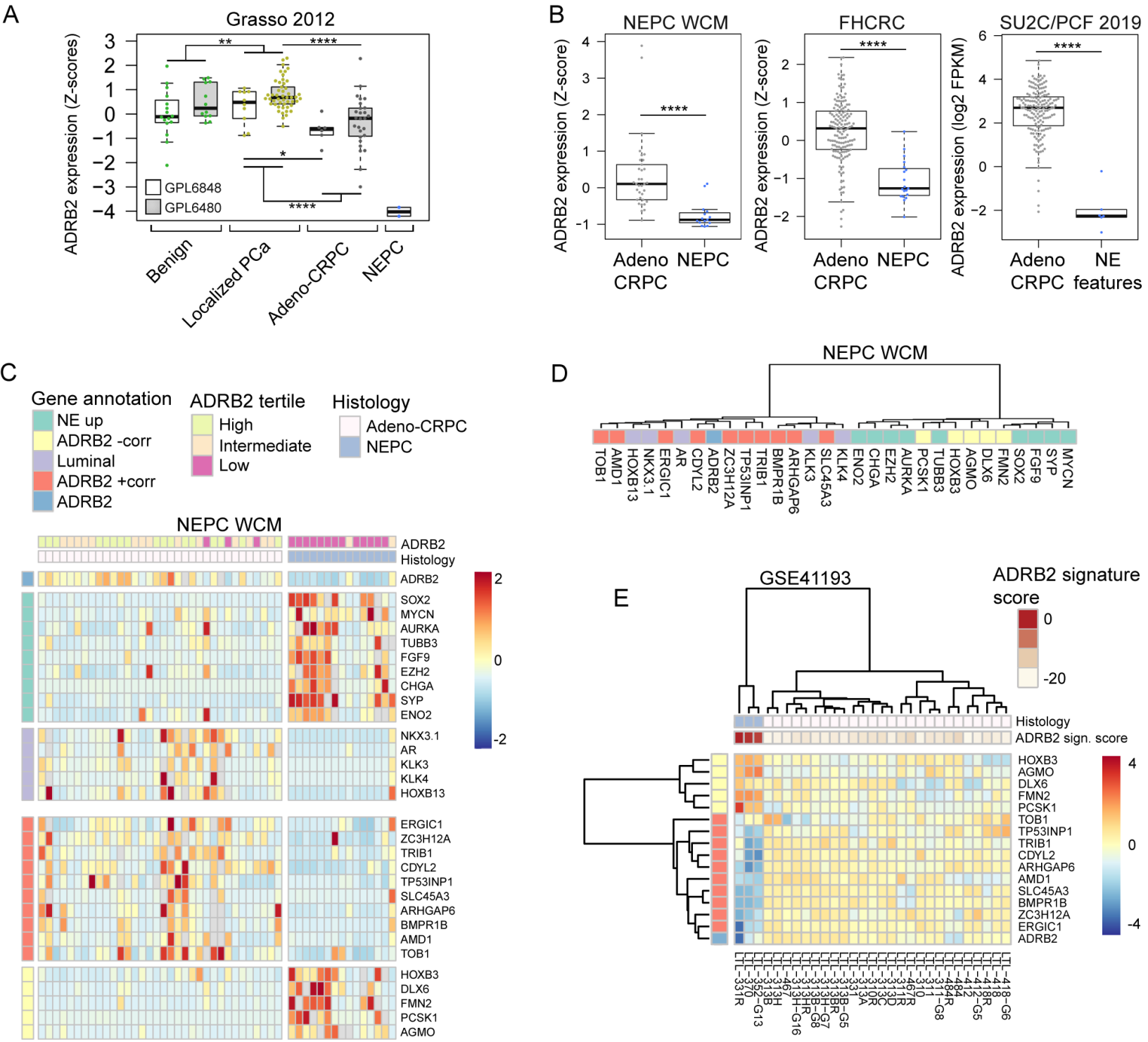
A
Grasso 2012
ADRB2 expression (Z-scores)
GPL6848
GPL6480
Benign
Localized PCa
Adeno-CRPC
NEPC
B
NEPC WCM
FHCRC
SU2C/PCF 2019
ADRB2 expression (Z-score)
ADRB2 expression (log2 FPKM)
Adeno CRPC
NEPC
NE features
C
Gene annotation
NE up
ADRB2 -corr
Luminal
ADRB2 +corr
ADRB2
ADRB2 tertile
High
Intermediate
Low
Histology
Adeno-CRPC
NEPC
NEPC WCM
ADRB2
Histology
SOX2
MYCN
AURKA
TUBB3
FGF9
EZH2
CHGA
SYP
ENO2
NKX3.1
AR
KLK3
KLK4
HOXB13
ERGIC1
ZC3H12A
TRIB1
CDYL2
TP53INP1
SLC45A3
ARHGAP6
BMPR1B
AMD1
TOB1
HOXB3
DLX6
FMN2
PCSK1
AGMO
D
NEPC WCM
TOB1
AMD1
HOXB13
NKX3.1
ERGIC1
AR
CDYL2
ADRB2
ZC3H12A
TP53INP1
TRIB1
BMPR1B
ARHGAP6
KLK3
SLC45A3
KLK4
ENO2
CHGA
EZH2
AURKA
PCSK1
TUBB3
HOXB3
AGMO
DLX6
FMN2
SOX2
FGF9
SYP
MYCN
E
GSE41193
ADRB2 signature score
Histology
ADRB2 sign. score
HOXB3
AGMO
DLX6
FMN2
PCSK1
TOB1
TP53INP1
TRIB1
CDYL2
ARHGAP6
AMD1
SLC45A3
BMPR1B
ZC3H12A
ERGIC1
ADRB2

Figure 6

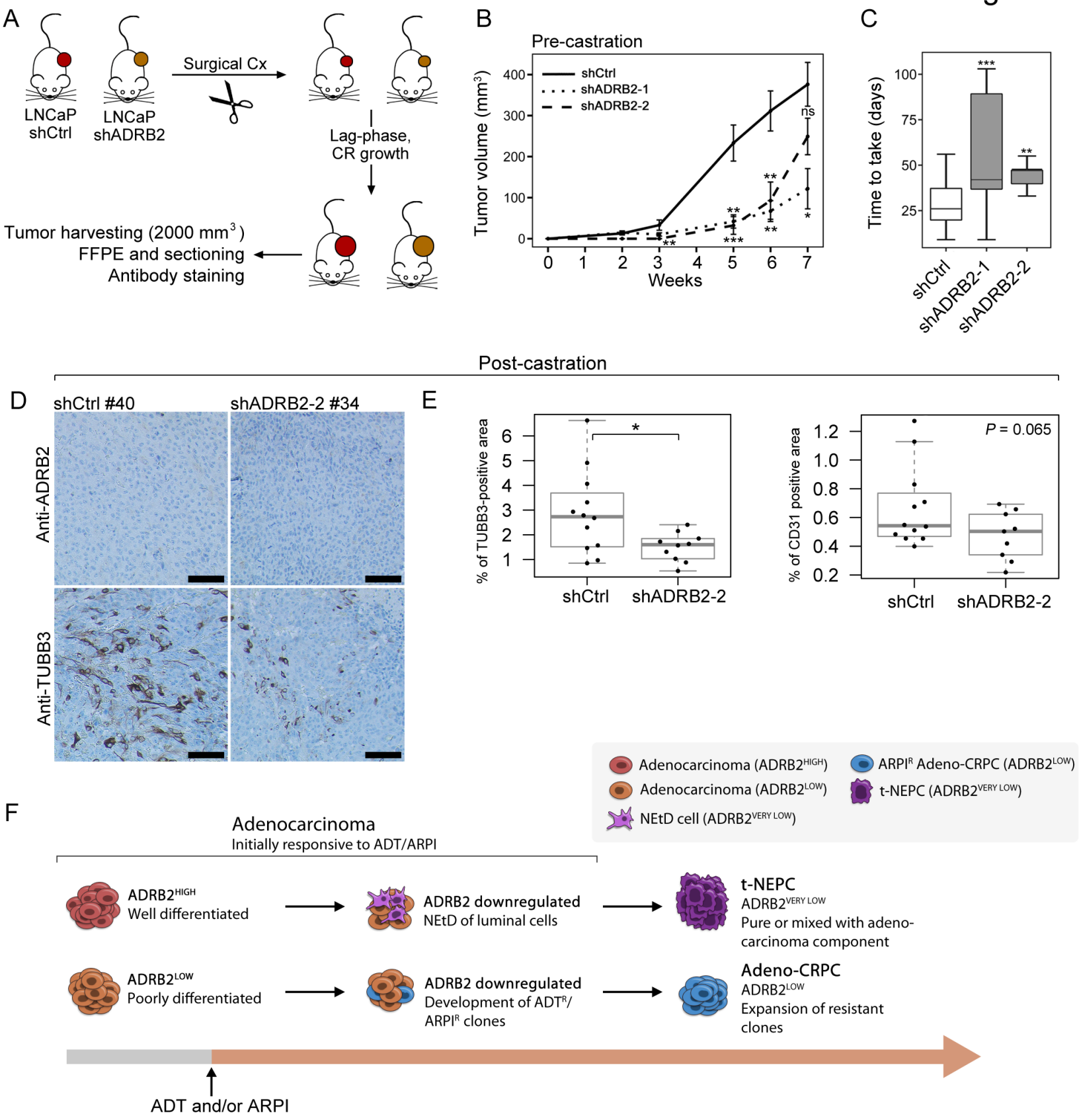
A
LNCaP shCtrl
LNCaP shADRB2
Surgical Cx
Lag-phase, CR growth
Tumor harvesting (2000 mm3)
FFPE and sectioning
Antibody staining
B
Pre-castration
shCtrl
shADRB2-1
shADRB2-2
Tumor volume (mm3)
Weeks
ns
C
Time to take (days)
shCtrl
shADRB2-1
shADRB2-2
Post-castration
D
shCtrl #40
shADRB2-2 #34
Anti-ADRB2
Anti-TUBB3
E
% of TUBB3-positive area
shCtrl
shADRB2-2
% of CD31 positive area
P = 0.065
Adenocarcinoma (ADRB2HIGH)
Adenocarcinoma (ADRB2LOW)
NEtD cell (ADRB2VERY LOW)
ARPIR Adeno-CRPC (ADRB2LOW)
t-NEPC (ADRB2VERY LOW)
F
Adenocarcinoma
Initially responsive to ADT/ARPI
ADRB2HIGH
Well differentiated
ADRB2 downregulated
NEtD of luminal cells
t-NEPC
ADRB2VERY LOW
Pure or mixed with adeno-carcinoma component
ADRB2LOW
Poorly differentiated
ADRB2 downregulated
Development of ADTR/ ARPIR clones
Adeno-CRPC
ADRB2LOW
Expansion of resistant clones
ADT and/or ARPI